Ph.D. DISSERTATION

Enhancement of viewing characteristics of depth-fused display with autostereoscopic display and projection-type display technologies

무안경식 3 차원 디스플레이와 투사형 디스플레이를 이용한 깊이 융합 디스플레이의 관찰 특성 향상

BY

Soon-gi Park

AUGUST 2015

DEPARTMENT OF ELECTRICAL ENGINEERING AND
COMPUTER SCIENCE
COLLEGE OF ENGINEERING
SEOUL NATIONAL UNIVERSITY

Ph.D. DISSERTATION

Enhancement of viewing characteristics of depth-fused display with autostereoscopic display and projection-type display technologies

무안경식 3 차원 디스플레이와 투사형 디스플레이를 이용한 깊이 융합 디스플레이의 관찰 특성 향상

BY

Soon-gi Park

AUGUST 2015

DEPARTMENT OF ELECTRICAL ENGINEERING AND
COMPUTER SCIENCE
COLLEGE OF ENGINEERING
SEOUL NATIONAL UNIVERSITY

Enhancement of viewing characteristics of depth-fused display with autostereoscopic display and projection-type display technologies

무안경식 3 차원 디스플레이와 투사형 디스플레이를 이용한 깊이 융합 디스플레이의 관찰 특성 향상

지도교수 이 병 호

이 논문을 공학박사 학위논문으로 제출함

2015 년 5 월

서울대학교 대학원

전기 컴퓨터 공학부

박 순 기

박순기의 공학박사 학위논문을 인준함

2015 년 6 월

위 원 장 _____

부위원장 _____

위 원 _____

위 원 _____

위 원 _____

Abstract

Enhancement of viewing characteristics of depth-fused display with autostereoscopic display and projection-type display technologies

SOON-GI PARK
DEPARTMENT OF ELECTRICAL ENGINEERING AND
COMPUTER SCIENCE
COLLAGE OF ENGINEERING
SEOUL NATIONAL UNIVERSITY

In this dissertation, various methods for enhancing the viewing characteristics of the depth-fused display are proposed with combination of projection-type displays or integral imaging display technologies. Depth-fused display (DFD) is one kind of the volumetric three-dimensional (3D) displays composed of multiple slices of depth images. With a proper weighting to the luminance of the images on the visual axis of the observer, it provides continuous change of the accommodation within the volume confined by the display layers. Because of its volumetric property depth-fused 3D images can provide very natural volumetric images, but the base images should be located on the exact positions on the viewing axis, which gives complete superimpose of the images. If this condition is not satisfied, the images are observed as two separated images instead of continuous volume. This viewing characteristic extremely restricts the viewing condition of the DFD resulting in the limited applications of DFDs.

While increasing the number of layers can result in widening of the viewing angle and depth range by voxelizing the reconstructed 3D images, the required system complexity also increases along with the number of image layers. For solving this problem with a relatively simple configuration of the system, hybrid techniques are proposed for DFDs. The hybrid technique is the combination of DFD with other display technologies such as projection-type displays or autostereoscopic displays. The projection-type display can be combined with polarization-encoded depth method for projection of 3D information. Because the depth information is conveyed by polarization states, there is no degradation in spatial resolution or video frame in the reconstructed 3D images. The polarized depth images are partially selected at the stacked polarization-selective screens according to the given depth states. As the screen does not require any active component for the reconstruction of images, projection part and reconstruction part can be totally separated. Also, the projection property enables the scalability of the reconstructed images like a conventional projection display, which can give immersive 3D experience by providing large 3D images. The separation of base images due to the off-axis observation can be compensated by shifting the base images along the viewer's visual axis. It can be achieved by adopting multi-view techniques. While conventional multi-view displays provide different view images for different viewer's positions, it can be used for showing shifted base images for DFD. As a result, multiple users can observe the depth-fused 3D images at the same time. Another hybrid method is the combination of floating method with DFD. Convex lens can optically translate the depth position of the object. Based on this principle, the optical gap between two base images can be extended beyond the physical dimension of the images. Employing the lens with a short focal length, the gap between the base images can be greatly reduced. For a practical implementation of the

system, integral imaging method can be used because it is composed of array of lenses. The floated image can be located in front of the lens as well as behind the lens. Both cases result in the expansion of depth range beyond the physical gap of base images, but real-mode floating enables interactive application of the DFD. In addition to the expansion of depth range, the viewing angle of the hybrid system can be increased by employing tracking method. Viewer tracking method also enables dynamic parallax for the DFD with real-time update of base images along with the viewing direction of the tracked viewers. Each chapter of this dissertation explains the theoretical background of the proposed hybrid method and demonstrates the feasibility of the idea with experimental systems.

Keywords: Autostereoscopic three-dimensional display, depth-fused display, projection-type display, polarization-encoding, integral imaging, multi-view display, accommodation response, viewer tracking

Student Number: 2011-30233

Contents

List of Figures

List of Tables

Chapter 1

Introduction

1.1 Overview of three-dimensional displays

Three-dimensional (3D) displays have been researched more than hundred years, and with the rapid growth of the electronic displays and imaging devices, they are also developed explosively for last two decades [1]. In these days, 3D displays are considered as next generation displays combined with computer graphic technologies such as virtual reality (VR) or augmented reality (AR). 3D displays are of interest for a long time because the viewing process of 3D displays is very similar to the that of real world resulting in provision of more natural viewing experience to observers. It gives more realistic and immersive experience beyond the space and time limit.

In the real world, a human observes a 3D object by using several depth cues, which include physiological change of the human visual organs [2]. Some other cues which do not induce the physiological changes are called as psychological or pictorial cues, because they can be expressed on a two-dimensional (2D) plane.

For example, shade, occlusion or relative size of the object can give the depth information. Those cues are usually empirically obtained. Binocular disparity is the difference of the perceived image in each eye due to the position difference of the eyes. Convergence is the rotation of the eye balls in the socket for directing the eyes to the object. According to the distance of an object, the eyes rotate inward (near) or outward (far). Accommodation is the change of focal length of the lens in the eye. The lens becomes thicker when the object is located near, and vice versa. Theses three depth cues are very closely related because they usually happens at the same time. The change of one of these depth cues induces the change of the others [3]. Because of this relationship between the physiological depth cues, it gives uncomfortable feeling resulting in nausea, head ache or visual fatigue when those cues are mismatched [4]. Motion parallax is another important depth cue, although it does not induce the physiological change of human organs. It is the change of image aspect according to the position difference. For example, if the viewer moves the position to the right, the right side of the object is shown to the viewer, and vice versa.

Because psychological cues can be easily provided as shown in paintings or photographs, it is important to give physiological depth cues in 3D displays. Consequently, 3D displays try to reproduce the visual process in natural condition by replicating the depth perception procedure, but the technological limit restricts several factors making perfect 3D displays. Conventionally, most of the 3D displays exploit binocular disparity and vergence because they are most dominant factors in the near viewing condition, which is the distance less than 10 meters [2, 5]. Over that distance, pictorial depth cues like relative sizes, airy blur, or occlusion become more dominant.

3D displays can be categorized according to the main principles of the system, which contribute to the 3D perception. Most of them are based on image

rays or directional views, which are the images that can only be observed at the specific direction or location. In order to make directional view images, various optical technology is used. The simplest method is using an optical filter, usually glasses-type, in front of the eyes so that different directional view images are filtered to each eye. This kind of 3D system is called stereoscopic 3D displays, and it is the most common 3D system in TV market and theater [6]. Currently, wavelength (or color), polarization, or alternating shutter glasses is most commonly used for filtering left and right directional views. Spatially separated two displays located in front of the eyes can also provide a stereoscopic 3D image. These kinds of displays are called head-mounted displays (HMDs). Recently, they are getting spotlights because of their immersive 3D experience with wide coverage of human visual field [7, 8]. Directional-view-based displays do not require complexed system, but the lack of other depth cues such as accommodation results in uncomfortable viewing experience causing visual fatigue.

If the optical components are attached on the display instead of the human eyes, observers can more comfortably enjoy 3D images without wearing encumbering viewing-aids. This kind of system is called autostereoscopic 3D displays. For the optical component, parallax barrier, pin-holes or lens array are commonly used with flat-panel displays such as liquid crystal displays (LCDs) or organic light-emitting diodes(OLEDs). Recently, thanks to the development of display technology, the performance of the display system is greatly increased resulting in dynamic pin-holes or parallax barriers, which can greatly increase the viewing quality of the autostereoscopic displays [9, 10]. Also, the light field [11], which is a set of directional light rays, analysis of the view image results in a compressive display, which generalizes the parallax barrier into an optical transparency [12, 13]. It can achieve high resolution autostereoscopic 3D display by

optimizing light field according to the displays system with various optical and computational techniques [14,15]. However, autostereoscopic displays also suffer from the visual fatigue due to the lack of accommodation cue.

Volumetric displays are 3D displays composed of volumetric pixels called voxels. Voxels are distributed in the 3D space and shows specific color information. Volumetric displays represent perfect 3D images which satisfy all of the depth cues, but the reproduced images are confined in a specific volume that is covered by the display in most of the systems. The simplest and most intuitive volumetric display is a light emitting diode (LED) cube, whose voxels are made of LEDs, but the required number of LEDs increases exponentially as its volume grows. Because of this problem, voxels are made by afterimage effect with a volume sweeping screen with optical or mechanical method [16–18]. In case of the mechanical movement of the screen, the screen entails the noise, and safety windows are essential for safe observation of the object. Another problem from which volumetric display suffers is the incorrect occlusion. Because voxels emit light in every direction regardless of their position, the occlusion can not be correctly represented, and images are transparent without solving this problem.

Holography is a different approach to the 3D displays because it is based on the wave optics rather than ray optics. It uses the interference and diffraction property of the light wave, while other 3D displays are based on ray optics. However, updatable holographic medium does not show good performances currently [19]. Digital holographic displays, which can be made by electronic devices such as a spatial light modulator, require tremendous amount of information, which is even higher than the full-parallax 3D displays. Holographic displays can perfectly reconstruct a light wave propagating in the space which satisfies every depth cues, but technological development of display device and

computing performance is still not enough to provide real-time hologram with natural viewing conditions. Some holographic displays adopted spatial multiplexing and tracking method in order to provide wider viewing angle [20], but detailed principle of the system is beyond the scope of this dissertation.

Table 1.1 3D display methods and supported depth cues

Depth cues	*Display methods*
Binocular disparity	Stereoscopic, autostereoscopic, volumetric, holographic
Vergence	Stereoscopic, autostereoscopic, volumetric, holographic
Accommodation	Volumetric, holographic
Motion parallax	Autostereoscopic, volumetric, holographic

As shown in the Table 1.1, most of the current 3D displays do not support all depth cues. Only volumetric displays and holography can satisfy the all depth cues but they require complexed system configurations and tremendous amount of data. Some of the autostereoscopic displays can satisfy accommodation cues, but they sacrifice some of the viewing qualities such as spatial resolution, because of the trade-off relationship among the viewing parameters. Simply, one pixel in the display corresponds to one ray in a 3D display, and the distribution and density of the ray bundles defines the other parameters such as resolution, viewing angle, or depth range. It is very hard to overcome the spatial bandwidth product limit with a conventional method. Compressive display method is considered as a candidate that can break the data capacity limit by using the correlation between directional view images, but it still requires very dense ray bundles to provide accommodation cues [21].

It is known that accommodation response can be induced in a directional-view-based 3D display when two view images are incident on one eye. It is known as a super multi-view condition, and it has been demonstrated by many

experimental results [22–26]. Although it provides very natural 3D images due to the provision of all physiological depth cues, it requires tremendous amount of data and system resources, which make the system bulky and complicated [27–29]. The narrow spacing between the directional views reduces the size of viewing zone and viewing angle. Or if the size of viewing zone is conserved the resolution of each view image is greatly reduced without increasing the system resources. However, they are considered as a promising bridge from the current stereoscopic 3D system to the ultimate 3D displays such as large scale volumetric displays or electronic hologram.

1.2 Motivation

In this dissertation, the volumetric characteristics of the 3D display are in focus, which can provide very natural 3D image with full support of physiological depth cues in a wide range of viewing zone. Current problems, which are occlusion, confined volume, and so forth, of the volumetric displays originate from the property of the voxels. If the voxels can be observed only in one direction like directional view images, it can solve the occlusion problem. In that case, only the outer most voxels are observed, and it becomes the 3D surface of the object and reduces the required amount of information [30]. Volumetric displays which consist of stack of plane images have this kind of directional volumetric characteristics. By applying proper weight of plane images results in continuous depth representation although planes are separated. It is called depth-fusing effect, and a 3D display based on this principle is called a depth-fused display [31]. Depth-fused displays are also called depth-fused 3D displays, multi-focal displays, or multi-layer displays. The principle of depth-fusion has been analytically and clinically proven that proper depth blending results in continuous accommodative response between the planes [31–34]. Generally, the depth position is decided by the linear luminance weight of the accommodative distance represented by diopter (D, 1/m) as shown in Fig. 1.1. Because depth-fusion occurs properly within the depth-of-field of the eye, which is 0.6D, the gap between two planes should be less than 0.6D [33]. As the depth range is represented in a reciprocal of the physical distance, this range can be infinite if the viewing distance is more than 1.67 m (0.6D).

However, the depth blending requires exact superposition of two plane images along the visual axis. Otherwise, the plane images are not fused, and they are observed as separated two images. For solving this problem, multi-

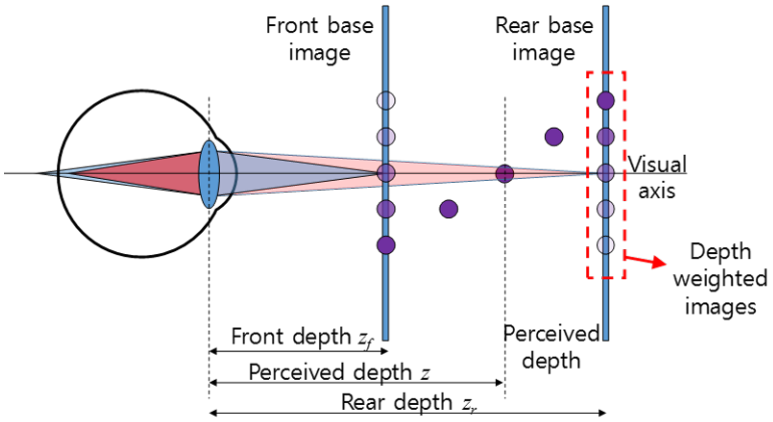

Figure 1.1 Accommodation of the depth-fused display according to the luminance weight of the plane

projection method or tracking method have been proposed to compensate the viewer's, movement [35,36]. The previous studies proposed that the viewing condition of the DFD can be improved by employing other display technologies like projection displays rather than using flat-panel displays. In this dissertation, combination methods of depth-fused display with other display technology are proposed for overcoming the limitation of depth-fused display. With expansion of depth-fused displays by combining other display technologies, the viewing condition can be greatly improved as well as the expressible depth range or other 3D image characteristics. Also, the physical dimension of the system can be reduced by optical translation of the depth position while conventional volumetric displays require large volume in order to represent a large object.

1.3 Scope and organization

This dissertation contains the explanation of depth-fused display techniques, which are combined with other display technologies for the improvement of viewing characteristics or quality of the provided 3D images. Each chapter explains the basic idea and principle of the system, and demonstrates the feasibility with experimental prototype system. In Chapter 2, projection-type DFD system is proposed with the concept of the polarized-depth images. By projecting the polarization-encoded image, scalable 3D image can be provided with polarization-sensitive screen. The system can be implemented by attaching depth modulator in the conventional projection display. Chapter 3 describes the principle of flat-panel based DFD with extended depth range and wide-viewing angle. By adopting integral imaging and multi-view techniques to a DFD system, it can provide larger depth range compared to the conventional DFDs, which only provide 3D images between the stacked panels. The viewing angle, which is extremely restricted in the conventional system, can be also enhanced by the principle of multi-view display. Chapter 4 introduces the further improvement of the flat-panel-based DFDs by adopting integral imaging and tracking method. By using the real-mode integral imaging technique, the system can generate a 3D image out of the display system, which is very challenging in the conventional DFD systems. Also, the viewing angle of the system is widened by adopting viewer-tracking system. The tracking also enables the realization of parallax images which is difficult to provide with the conventional systems. The dissertation will be summarized in chapter 5, and research topics for further improvement of the system will be also discussed.

Chapter 2

Multi-layered depth-fused display with projection-type display

2.1 Introduction

The multiplexing method employed to add 3D information to a 2D scene is indispensable to achieve a 3D display system providing the appropriate depth cues. For example, a stereoscopic 3D display using polarization glasses produces the sensation of depth via binocular disparity, which is induced by the orthogonality of the polarization through two spatially or temporally multiplexed scenes for the left and right eye images [1, 37]. An autostereoscopic 3D display can be regarded as a system using a spatial multiplexing method that presents several directional scenes created by overlapping pixels through a lenticular lens, a parallax barrier, or some other optical element [1, 38]. Volumetric 3D displays using a spinning screen or scanned volume can be classified as systems using the time multiplexing method [17, 39]. Even holographic displays can be classified as systems that use the phase pattern as the additional dimension for

depth multiplexing, which requires analogue media or analogue modulators for achieving high-quality images [19, 40, 41]. These multiplexing methods require supplemental equipment, such as special viewing aids or a coherent light source, or they expend and deplete the limited system resources, such as the image resolution or driving frequency, which results in a conflict among the depth cues and degradation of the viewing quality of the represented 3D images [4]. In this chapter, a novel multiplexing method for a 3D display is introduced, the Lamina 3D display, which adopts the polarization ratio to provide depth information. The proposed system utilizes the modulation of the intensity ratio of the horizontal and vertical polarization (or rotations of the linear polarization) to encode the depth information; this method contrasts previous systems that use the polarization multiplexing method to exploit only the orthogonality of the polarization [42–44]. In the following sections, we describe how the proposed system can provide natural 3D information satisfying all of the essential depth perception cues – binocular disparity, vergence, accommodation, and motion parallax – with a relatively small amount of data (consisting of the information of a grayscale depth map based on only one-third of the conventional 2D image data) using a special laminated volume. Compared to the DepthCube 3D display introduced by LightSpace Technology [17], which has a multi-layer configuration similar to that of the Lamina 3D display, the proposed polarization-based depth-encoding method has a superior viewing quality because it does not degrade the color expression, spatial resolution, or video frame rate. These characteristics distinguish the proposed system from previous volumetric 3D displays based on time multiplexing methods, including the DepthCube [17, 39, 45]. We also propose two types of systems according to the decoding method used to obtain the polarized depth information, each of which demonstrates unique advantages, using passive and active polarization-sensitive

optical components.

2.2 Polarization-encoded depth information for depth-fused display

The system is composed of projection part and imaging part like a conventional 2D projection display. However, the depth information in encoded as a polarization in the projection part, and the imaging part is composed of polarization sensitive screens. In the encoding part, the 2D scene is overlaid with the depth information modulated by a polarization-distributed depth map (PDDM), and the decoding component corresponds to the location at which relief-like 3D images are reconstructed in the special volume created by the laminated layers using the illumination characteristics of the polarization dependence of each layer. Conceptual diagrams illustrating the configuration and principle of the Lamina 3D display are presented in Fig. 2.1.

The encoding component of the Lamina 3D display can be implemented using a simple 2D projector and spatial light modulator (SLM), such as a twisted nematic-liquid crystal display (TN-LCD), which can rotate the polarization state of each pixel according to the grayscale of the input depth image [46]. Consequently, two SLMs are needed for the encoding component: one for 2D imaging and another for depth encoding. The 2D image modulated by the PDDM can be easily obtained and does not experience temporal or spatial degradation during the depth multiplexing process because only the polarization of the image is modulated. The decoding component consists of polarization-sensitive optical devices. Because the human eye cannot detect the polarization of light but can detect the intensity of light, the special volume in which the polarization status is converted to the expressive depth must be defined within the decoding

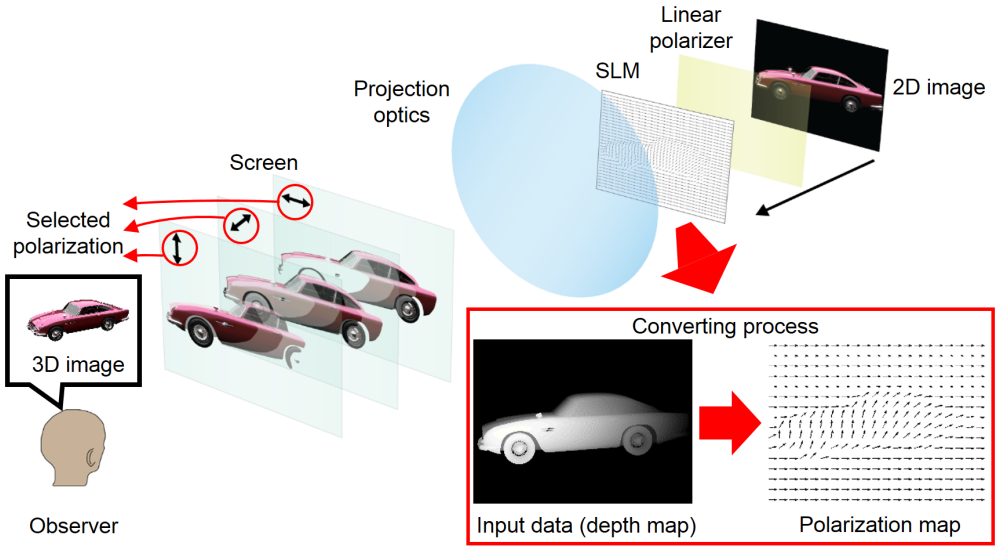

Figure 2.1 Conceptual diagram of the system configuration of the Lamina 3D display[2]

component of the Lamina 3D display. The special volume can be instrumented by laminating the volume with layers that can control the scattering and transmission ratio according to the polarization state of the projected light. We propose passive-types of Lamina 3D displays, of which the volume consists of multiple layers of scattering polarizer films, which scatter and transmit the incident light according to the angle difference between the polarization axes of the light and the films. The encoding component of the Lamina 3D display system can be assembled from SLMs for the 2D imaging and depth encoding, linear polarizers, and relay optics, including a projection lens set. The image from the SLM for the 2D imaging passes through the linear polarizer to ensure that the polarization state of the image is aligned with respect to the initial state

[2]The car 3D object in the figure is modeled by Natman and licensed under Creative Commons Attribution 3.0

for the modulation of the second SLM. To enable a pixel-wise modulation of the polarization, the pixels of the 2D image should be overlaid with the corresponding pixels of the polarization-modulating SLM. For this purpose, the relay optics must be placed between the SLMs or on the projection optics behind the SLM for the 2D image. The polarization status of each pixel of the projected image is modulated according to the grayscale of the corresponding pixel of the depth map by the second SLM, which works as a polarization rotator composed of a TN-LCD with the polarizers on both sides are removed. The input depth information of the second SLM is an 8-bit grayscale image with only one-third of the conventional 2D color information. This reduction in data is beneficial for the system implementation and information processing, including the acquisition and display processes. The modulation range is identical to the depth resolution, and it can be further improved by adopting an SLM which can modulate the polarization with more precise steps. After passing the second SLM, the image has various polarization angles for each pixel distributed from 0° to 90° according to the given depth information of the second SLM. In our experimental setup, 0° corresponds to the farthest depth and 90° is assigned to the nearest depth position. For the depth and image modulation, several types of SLMs can be used in this system. Generally two types of SLMs can be used for the 2D imaging SLM: digital micro-mirror devices (DMDs) or liquid crystal (LC) SLMs. In the case of the DMD-type SLMs, the SLM performs binary modulation so that the color and grayscale of the images are obtained by temporal multiplexing [47]. These characteristics may result in a temporal flickering interference with the switching screens in the active-type system. However, the DMD-type SLMs do not alter the polarization state of the image. Thus, the polarization modulation of the LCD can be directly performed after the relay optics have been passed. For the case of LC-type SLMs, the grayscale

information is obtained using the polarization, and the color of the image is achieved by combining three monochromatic SLMs with backlights consisting of the primary colors [48]. However, the different colors do not have the same polarization state. Thus, additional processing is required for the polarization modulation of the depth. The output image of the LC-type SLM has linear polarization; although the direction of the polarization is different, the output polarization of the SLMs can be converted to the identical circular polarization by a quarter-wave plate. Using this technique, the circular polarization can be used to reduce the influence of the polarization modulation of the depth in the LC-type SLM. By inserting another linear polarizer just before the second SLM for polarization encoding, the incoming polarization is calibrated to the initial state of the polarization modulation, and identical polarization modulation can be performed for each color, as achieved by the system with the DMD-type 2D imaging SLM.

2.3 Visualization with passive scattering film

The decoding component of the Lamina 3D display is the laminated volume, where the image encoded by the PDDM is represented by a relief-like 3D image. The relief-like 3D image is a set of voxels located in the outermost part of the object such that each pixel of the image requires only one depth value. With the relief-like representation of the 3D object, the 3D data can be effectively reduced using, for example, the hidden point removal method while preserving the 3D volumetric characteristics [30, 49]. The volume created by the passive screen is composed of arranged multiple scattering polarizers, whereas the active-type volume consists of stacked multiple PDLCs that can electrically switch between the transparent and scattering states by the application of an alternating current voltage. The specifications of the experimental setup of the system are summarized in Table 2.1. Another important characteristic of the Lamina 3D display is the number of laminated layers. A high number of layers is advantageous in this system because it widens the viewing angle and increases the depth perception within the expressible depth range [31, 34].

The proposed system has a simple configuration based on special polarizers that do not absorb but instead scatter the incident light according to the polarization angle. Because the polarization axes of the films are arranged rotationally, the amount scattered by each layer differs, producing the depth-directional intensity distribution for a certain polarization incidence. The change in intensity distribution in the depth direction can be observed as the difference in depth position. Therefore, the polarization-controlled image determined from the depth information can be represented as a relief-like 3D image. Figure 2.2 presents the basic scheme of the proposed system.

The results for the proposed system are shown in Fig. 2.3. In the figure,

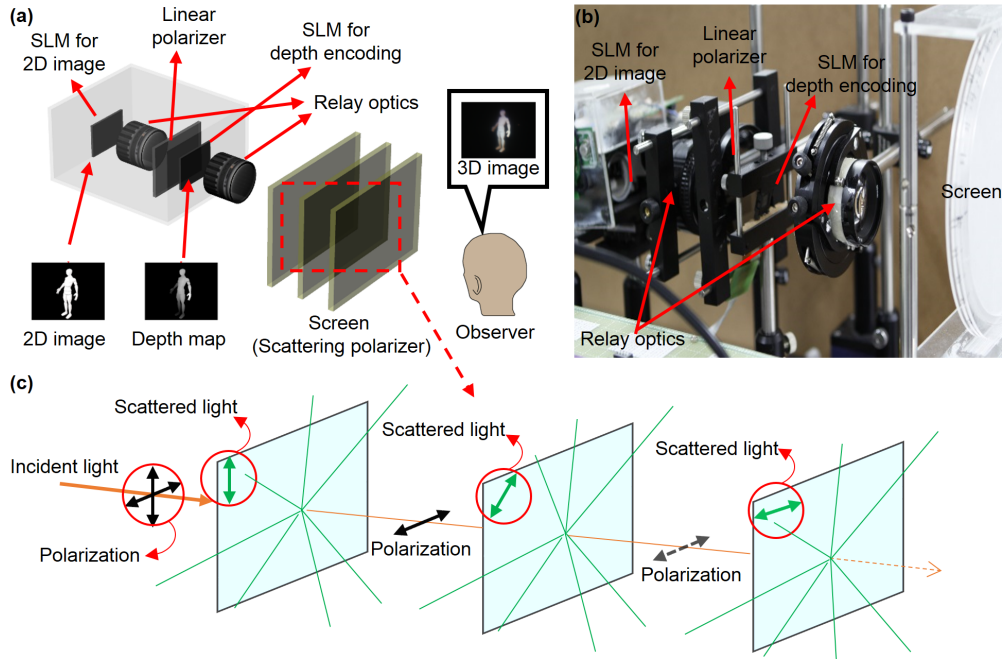

Figure 2.2 Schematic diagram of the experimental setup and prototype system. (a) Conceptual diagram of the system. The image generated by the SLM for 2D imaging passes through the linear polarizer in preparation for depth modulation. When the image passes through the SLM for depth encoding, which receives a grayscale depth image as an input, each pixel is modulated according to the input depth. (b) Prototype system. (c) Scattering process at each layer. The polarization-encoded depth image is projected onto screens consisting of scattering polarizers. The projected image is separated according to the encoded polarization, providing a 3D image to the observer.

stripe images used for depth calibration, simple geometric images, and car images are demonstrated, with side views demonstrating the parallax and reference depth images shown in the left column. The results indicate the feasibility of the proposed method with parallax in the side views. The decoding component of the proposed system has a succinct configuration and does not require a complicated implementation. This device can also achieve scalability using large scattering polarizers, as in conventional projection-type displays. However, the scattering property of the passive-type volume produces a haze in the reconstructed images. Because the general polarization is composed of two orthogonal components, the modulated polarization states cannot be perfectly separated from each other except in the orthogonal case. This behavior results in limited selectivity of the polarization and depth position, producing a blurry image that degrades the resolution of the reconstructed 3D image. The blur is aggravated if more scattering polarizers are inserted and sets a limit on the expressible depth range and viewing angles.

The scattering characteristics of the scattering polarizer can be expressed by the point spread function (PSF) depending on the input polarization angle. The PSF of one layer can be expressed as the Gaussian function shown in Eq. (2.1), whereas the PSF of the transmitted light is expressed by Eq. (2.2).

$$PSF_{S,\theta,\phi_{in}}(\theta,\phi) = a_S(\theta,\phi_{in}) \exp\left(-\frac{(\phi-\phi_{in})^2}{2b^2}\right), \tag{2.1}$$

$$PSF_{T,\theta,\phi_{in}}(\theta,\phi) = a_T(\theta,\phi_{in})\,\delta(\phi-\phi_{in}), \tag{2.2}$$

where θ represents the angle difference between the polarization state of the input light source and a scattering polarizer and ϕ is the deviation from the normal direction. ϕ_{in} represents the incident angle. $a_S(\theta,\phi_{in})$, $a_T(\theta,\phi_{in})$ and b

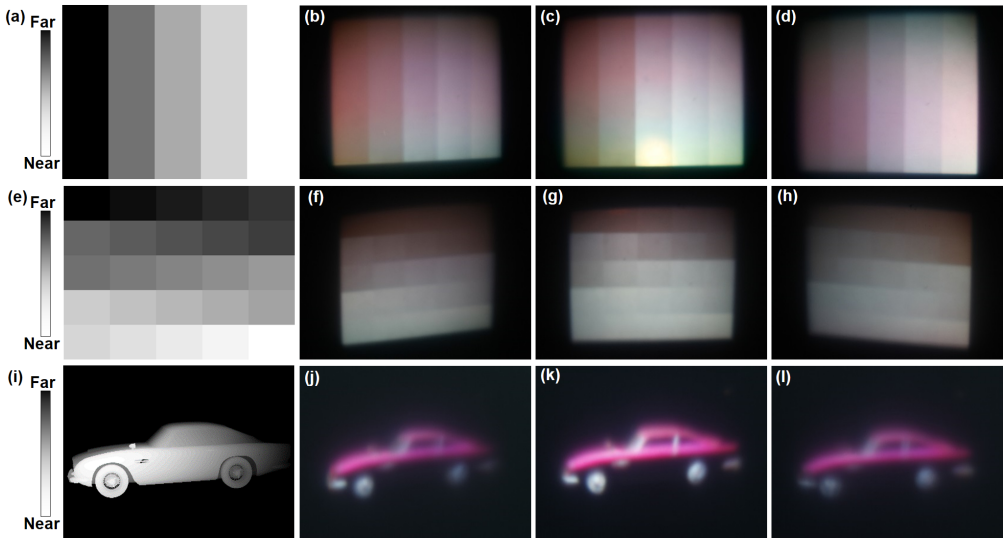

Figure 2.3 Resultant images of the Lamina 3D display. (a), (e), and (i) show depth images for calibration, abstract depth, and computer-generated 3D car images, respectively. (b), (c), and (d) show images from left, central, and right views of the reconstructed 3D images, respectively. (f), (g), and (h) show left, central and right views of the abstract depth image, respectively. (j), (k), and (i) show left, central and right views of the computer-generated 3D object, respectively.

are fitting parameters determined by the characteristics of the scattering polarizer and the conditions of the incident light ray. The coefficients a_s and a_t are highly dependent on the polarization state and incident angle, and their characteristics are estimated by measuring the property of the scattering polarizer. Because the scattering ratio of the light ray is a function of the angle difference between the polarization axes of light and the scattering polarizer, both the scattered portion and transmitted portion of the light should be included when calculating the depth position of the pixels. The image at each layer is calculated as shown in Eqs. (2.3) and (2.4), where $*$ represents the convolution operator. The experimental results of the images filtered by the scattering polarizer for each layer are shown in Fig. 2.4.

$$imageS_n = imageS_{n-1} * PSF_{S,\theta,\phi_{in}} + imageT_{n-1} * PSF_{S,90-\theta,\phi_{in}}, \quad (2.3)$$

$$imageT_n = imageS_{n-1} * PSF_{T,\theta,\phi_{in}} + imageT_{n-1} * PSF_{T,90-\theta,\phi_{in}}, \quad (2.4)$$

Thus, the observed images of each layer are transparency-weighted scattered images because the images are degraded as they pass through the layers. This behavior can be expressed as the following relationship in Eq. (2.5), where the transparency weight w_n is given by Eq. (2.6), R represents a rotation matrix, and α_n denotes the polarization axis of the n-th scattering polarizer.

$$imageI_n = w_n \quad \times \quad imageS_n, \quad (2.5)$$

$$w_n = \left\| \prod_{n}^{N} R(\alpha_n) PR(-\alpha_n) \right\|^2. \quad (2.6)$$

Finally, the reconstructed 3D image can be calculated by merging the retinal images of each layer with the calculated focusing position in Eq. (2.7) using

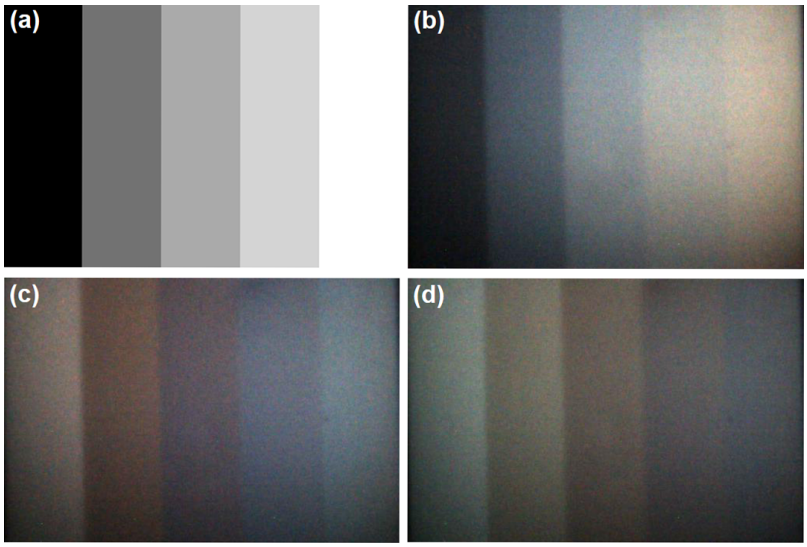

Figure 2.4 Filtered images at each layer of the system. (a) Depth information and (b) filtered image at the nearest layer, (c) middle layer, and (d) farthest layer. The scattering and transmitting portions of the image are shifted according to the angle difference between the polarization axes of the image and the screen.

the linear luminance weight [31, 34]. Thus, the amount of the degradation that occurs can be obtained from the degradation profile of the retinal image.

$$z\left(x,y\right) \cong \sum_{N} \frac{imageI_n\left(x,y\right) \times z_n}{\sum_N imageI_n\left(x,y\right)}. \tag{2.7}$$

Based on this analysis, the author simulates the blur characteristics of the three-layer Lamina 3D display. The author uses an Imajor scattering polarizer provided by Teijin DuPont (Japan), and the angular scattering characteristics of the scattering polarizer are measured with a luminance meter[3] for normal and oblique light incidence. The linearly fitted coefficients for Eqs. (2.1) and (2.2) are as follows:

$$\begin{aligned} a_S\left(\theta,\phi\right) &= \left(0.9 - 0.01\theta\right) \times \left(0.99 - 0.0082\phi\right), \\ b &= 8.46, \\ a_T\left(\theta,\phi\right) &= \left(0.01\theta\right) \times \left(0.99 - 0.0082\phi\right). \end{aligned} \tag{2.8}$$

After the passing the scattering polarizer, the polarization axis is aligned to the that of the previous layer. As a result the PSF of the scatted portion of the image decided by the angle difference of scattering axes between the adjacent layers. Figure 2.5 shows the PSF of the scattering polarizers according to the angle difference of the polarizers.

In the simulation, each layer is placed 4 mm from its neighbors, and the scatting axes of the scattering polarizer are 0°, 45°, and 90° in the order of the farthest to nearest layers with respect to the observer. The input image is the delta function, which has a width of one pixel. For the three cases of polarization corresponding to 0°, 45°, and 90°, the PSFs of the image are obtained under the focusing conditions of the observer according to the simulated depth calculated by Eq. (2.7). The resulting focusing positions are 7.6 mm, 5.2 mm, and 2.33

[3]LS-100, Konica Minolta

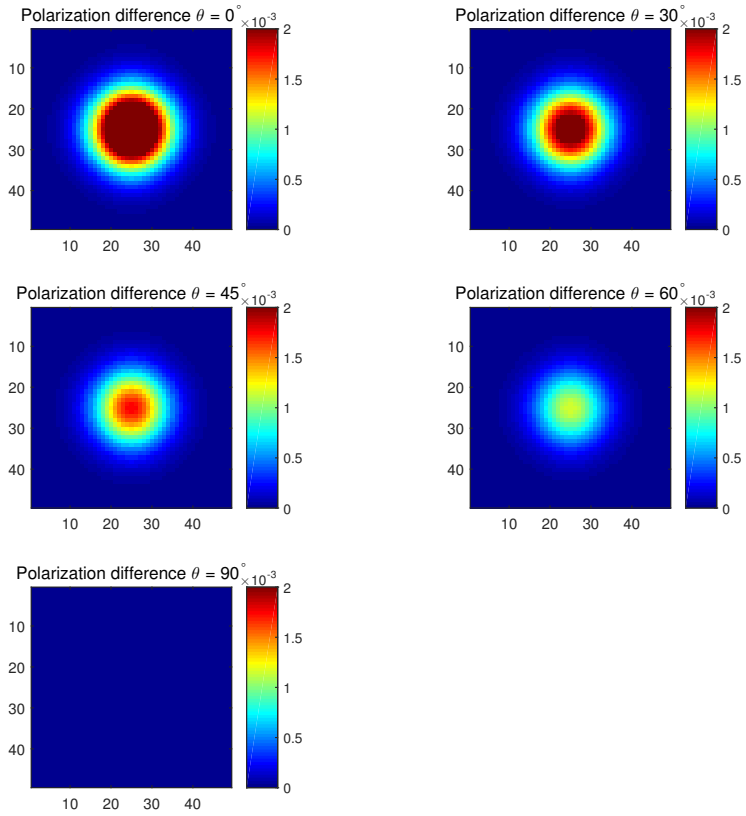

Figure 2.5 Point spread function of the scattering polarizer for various input polarization with normal incidence, $\phi_{in} = 0$, and without shift $\phi = 0$

mm for input polarizations of 0°, 45°, and 90°, respectively, and the nearest and farthest layers are located at 0 and 8 mm, respectively. The graph in Fig. 2.6 provides an example of the PSF for an input polarization of 45°. The author assumed that the PSF is circularly symmetric so that the 2D PSF can be obtained from the 1D profile of the PSF. Based on the calculated PSF, the author simulated a square image with a depth location set at the middle of the stacked layers. The input polarization was set to 45° to set the image at the middle layer.

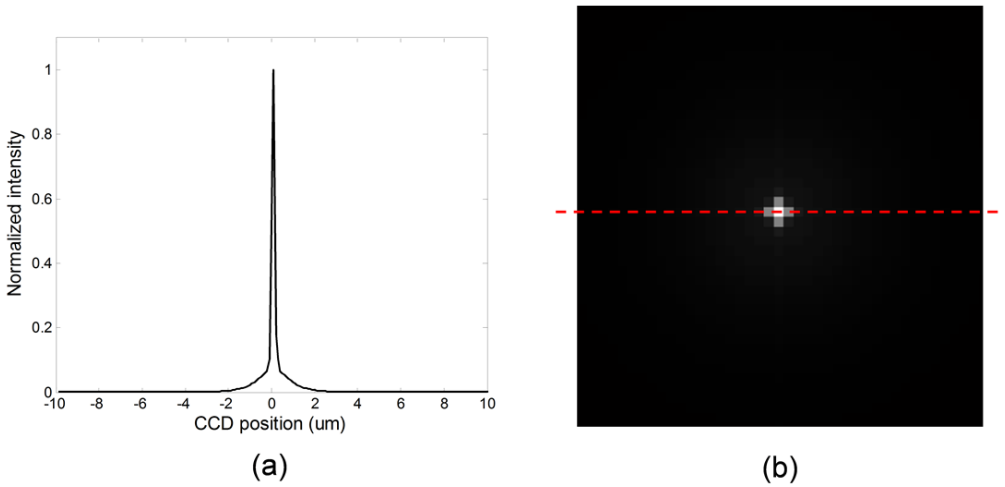

Figure 2.6 PSF of the Lamina 3D display with an input polarization of 45°. (a) 1D PSF of the system. The profile corresponds to the cross section of the 2D PSF along the red dashed line in (b). (b) 2D PSF of the system. The author assumed that the PSF is circularly symmetric, and the 2D PSF is obtained from the 1D PSF. The pixel pitch of the imaging device is assumed to be 1 μm. Thus, the 2D PSF presents a truncated image of the 1D profile.

Figure 2.7 shows the simulated result of scattering and transmitting images of three-layer Lamina display system having 0°, 45°, and 90° of polarization axis according to the input polarization angle. Because adjacent layers are dependent on each other, overall intensity of the image is decreased as the image passes

layers.

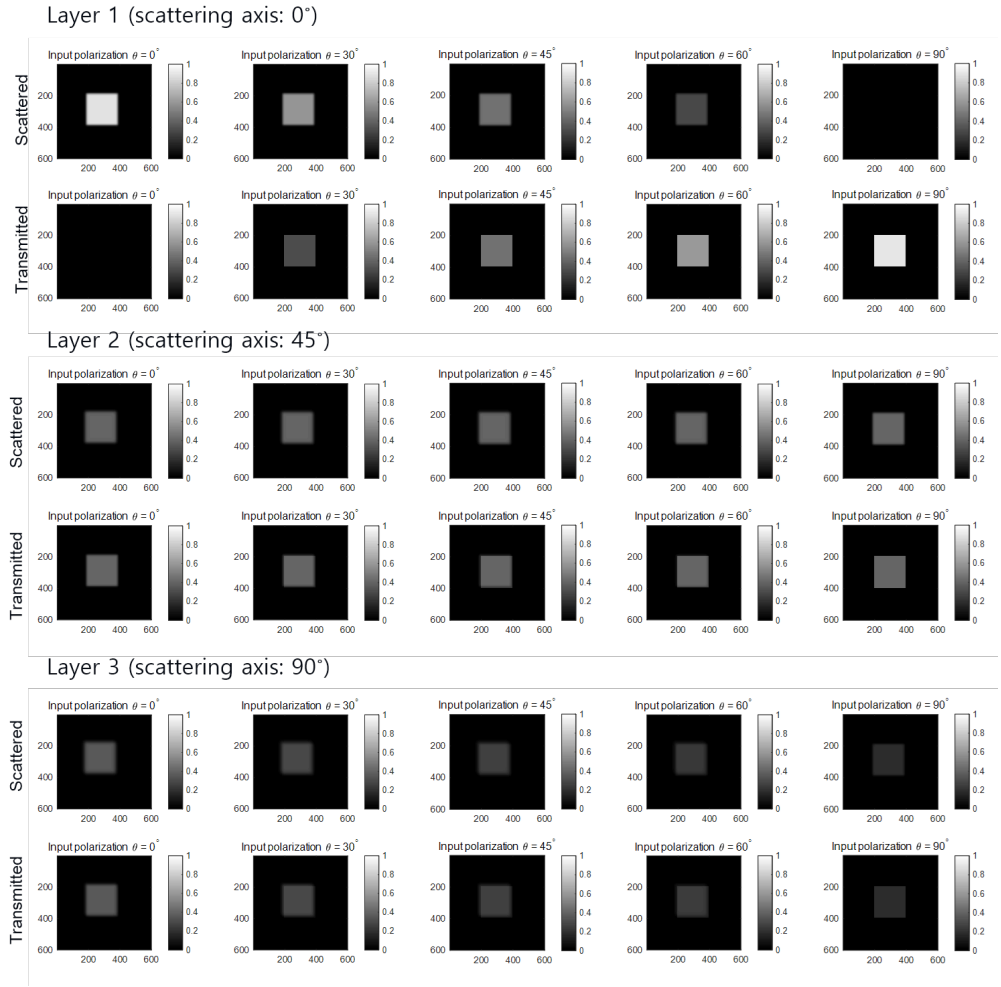

Figure 2.7 Scattering and transmitted portions of image at each layer

Figure 2.8 shows the relative depth position of the perceived images according to the modulated polarization angles. The relative depth position is calculated by the Eq. (2.7) with the depth position of layers in 1, 2 and 3 (arbitrary unit). As shown in the graph, imaging points with different polarization

states are perceived as points with different depths. However, the limited polarization selectivity results in shrinking of depth dimension. While the original depth range of the layers ranges from 1 to 3, the simulated results of the depth positions ranges from 1.9 to 2.4, approximately.

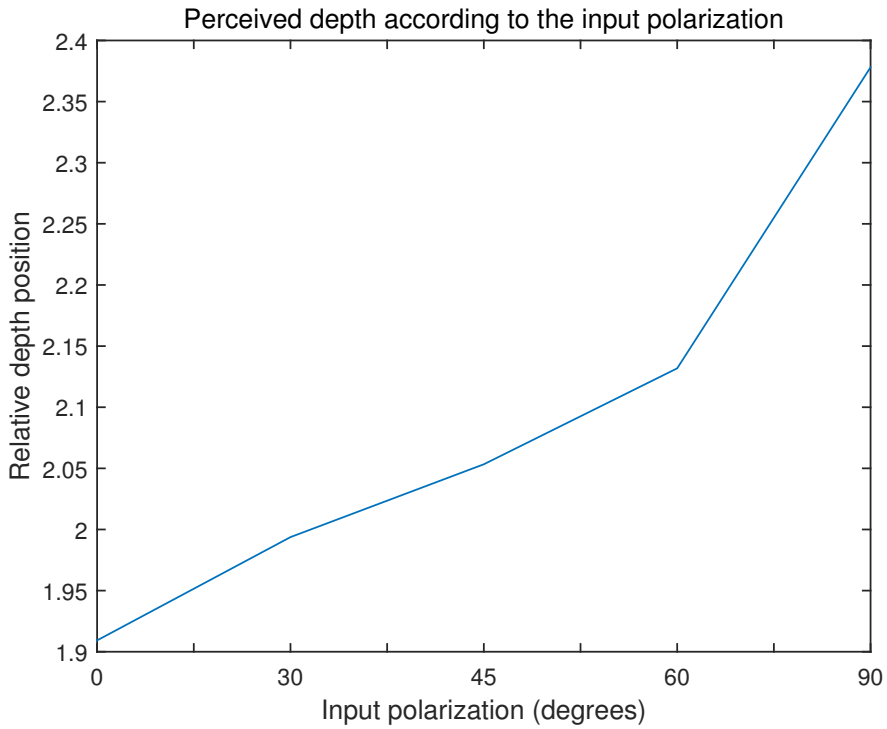

Figure 2.8 Simulation of the perceived depth position of images according to the input polarization angle

The simulated results are compared with the experimental results. The input 2D image is an entirely white square, as shown in Figs. 2.9(a) and 2.9(b). The blur observed for the experimental system is compared to the simulated data. For comparison, the images are normalized, and the difference between the original image and blurred image is determined to reduce the image noise or

offset of the experimental data. As shown in Fig. 2.9(g), the blur characteristics of the experimental and simulated results display similar trends. However, the image saturation, uneven uniformity, and oblique capturing direction of the imaging device result in a distortion of the blur characteristics.

Because the total PSF of the system becomes wider as more layers are inserted, the scattered images suffer from the aggravated blurring. The multiple scattering of the image can be expressed as multiple convolution of PSFs, of which the profiles are dependent on the angle difference of the scattering axis. Simple it can be shown as the following expression.

$$PSF = \mathcal{F}^{-1}\left\{\prod_{n=1}^{N}\mathcal{F}\left\{PSF_n\right\}\right\} \tag{2.9}$$

As shown in Fig. 2.10, the width of the curve becomes wider as the image passes the layers, which results in the aggravation of blurring of images as shown in the experimental results in Figs. 2.11(b) and 2.11(c). While the two-layer system does not suffer from the image degradation, the viewing angle of the system is severely limited. Also, the degradation of the image in systems having more than four layers suffered from the severe aggravation of blurring. As a result, the author compromises the number of layer as a three for achieving both wider viewing angle and decent image quality.

The author presents results for the experimental system with additional layers. Fig. 2.11 compares the reconstructed images based on the number of layers in the system. Although the systems with more layers achieve a wider viewing angle, the image degradation due to blurring becomes worse as the number of layers increases. Thus, there is a limitation to the number of layers that should be employed in the system.

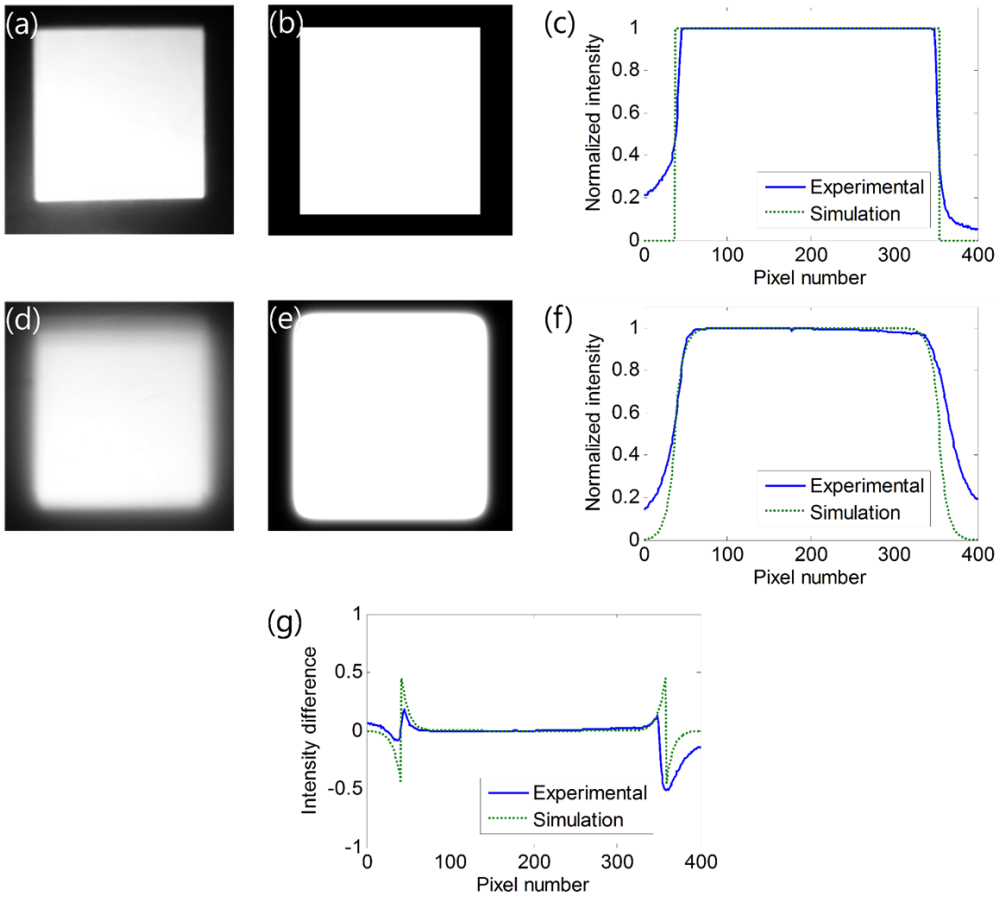

Figure 2.9 Comparison of the blur characteristics of the Lamina 3D display. The figures in the first row display the original images of a white square: experimental (a) and simulated (b) images and their horizontal intensity profiles (c). The figures in the second row display blurred images of the white square obtained with a three-layer configuration: experimental (d) and simulated (e) images and their horizontal intensity profiles (f). The input polarization angle is 45°, and the image is located at the middle layer. The difference between the original and blurred profiles of the images is shown in (g), indicating similar blur characteristics.

Table 2.1 Specification of the Lamina 3D display

	Parameters	
Encoding	2D imaging SLM (full color)	800 × 600 × 3 pixels
	Depth-encoding SLM (monochromatic)	800 × 600 pixels
Decoding	Screen type	Scattering polarizer
	Screen size	56 mm × 42 mm
	Number of layers	3
	Gap between layers	4 mm
	Total depth range	8 mm

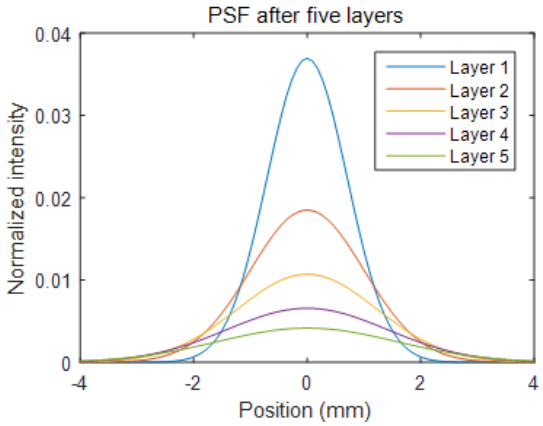

Figure 2.10 PSFs for a five-layer system whose optical axis is rotated 18° for each layer

Figure 2.11 Comparison of the image blur of the Lamina 3D displays according to the number of layers: (a) three layers, (b) four layers, and (c) five layers.

2.4 Summary

In this chapter, the author proposed a projection-type depth-fused display using polarization-encoded depth information. Projection-type 3D displays can provide immersive 3D experience with wide coverage of the human vision. By employing depth-modulating SLM and projection optics, the implemented DFD system can scale the reconstructed 3D images like a conventional projection-type display. The volumetric characteristics of the reconstructed images are beneficial for the multi-user applications with the realization of fatigue-free natural 3D image providing binocular disparity, vergence, accommodation and motion parallax. Also, the moderated amount of the data alleviates the computation load and transmission of information as well as the acquisition of 3D information using a depth camera. We expect that the proposed method can be applied to various applications which require a large-sized screen and moderate data such as tele-conference or broadcasting systems.

Chapter 3

Compact depth-fused display with enhanced depth and viewing angle

3.1 Introduction

Mobile display has become one of mainstreams in the current display market. It is natural that many researchers are focusing on the development of mobile 3D display. Current 3D mobile displays are focused on stereoscopic 3D displays, which are based on the prism-type or head-mounted-type method. The stereoscopic display, however, has limited applications such as virtual reality for gaming because visual-aid is essential to separate left and right images. The multi-view type autostereoscopic displays such as the lenticular type display and the parallax barrier type display are generally accepted as next-generation 3D displays [1, 50]. However, the multi-view type autostereoscopic display still has issues related with human factors at current level of technology. One of the main problems is the lack of comfortableness of a reconstructed 3D image caused by mismatching of the accommodation and the convergence. In this viewpoint,

the depth-fused display (DFD) is considered as a good solution of the problems for mobile 3D displays as it provides accommodation cue [31,33,34,51]. Because the DFD can provide accommodation, it is reported that the visual fatigue of reconstructed image is as small as that of two-dimensional (2D) displays [52]. The DFDs, however, have some limitations in depth-range and viewing angle. These weaknesses of the DFD originate from the condition of the depth-fusing effect. The depth-fusing effect is an adjustment of accommodation according to the luminance ratio of plane images of the DFD. The depth-fusing effect occurs when two images are overlapped. For this reason, if an observer moves out of the viewing position, overlapped images will be separated, resulting in the failure of depth-fusion. As a result, the narrow viewing angle of DFDs confines their applications to a single-observer display or a display with fixed viewing position. Because of this problem some kinds of DFD system were just used as two-depth display showing just two planar images without a depth-fusing effect [53, 54]. These kinds of display can provide images for multiple users, but it is hard to say that those systems are providing 3D images. In order to solve this problem, the two-view DFD was proposed using an anisotropic screen and a scattering polarizer [35]. It exploits polarization for separating the view of rear images. However, the use of polarization limits the further development of the number of views. For improving the viewing characteristics of the previous system, we proposed a DFD system with combination of other kinds of 3D displays for improving expressible depth range and providing more viewing positions, but those systems still have limitations in the expansion of viewing parameters [55, 56]. In this chapter, the author proposes a novel DFD that consists of virtual multi-view rear images and transparent front images. By inserting the optical element, the rear image can optically change its location according to the position of the observer, and it increases number of the viewing positions

of the system as well as the depth range without affecting the whole volume of the system, which is as compact as conventional DFDs. The feasibility of the proposed method is demonstrated using an experimental system.

3.2 Enhancement of viewing characteristics

3.2.1 Viewing angle enhancement using multi-view method

In this section, a method for improving the viewing qualities in the DFD is introduced. The basic concept is inserting an optical element such as a lenticular lens or a 2D lens array between the front and the rear layer of the DFD. By inserting an optical element, the system can give enhanced viewing characteristics because the rear image can be optically shifted according to directions of an observer, resulting in the prevention of image separation. The depth position of the image can also be optically translated to extend the depth range of the system. In these configurations, the front image of the DFD is fixed, while the rear image of the DFD is optically translated by the optical element according to the observer's viewing direction. Consequently, the fused 3D image can be shown in different viewing positions and have larger depth range. The schematic configuration of a system in comparison with a conventional system is shown in Fig. 3.1. While the conventional system shows separated front and rear images at an oblique viewing position like the observer 1 in Fig. 3.1(a), the proposed viewing-angle-enhanced system can provide correct depth-fused images to the multiple viewing points as illustrated in Fig. 3.1(b). When a lenticular lens is inserted, the lens and rear display panel can be considered as a conventional multi-view system. However, instead of showing multiple images having different parallaxes as in a conventional multi-view display, showing shifted-view images as depicted in Fig. 3.1(b) allows additional viewing points to DFD by preventing the image separation of the depth-fused image although the observer is not positioned at the exact front of the system.

For a natural depth-fusion of the front and the rear images, exact amount of shift should be calculated. For a rear image of the proposed system, horizontally

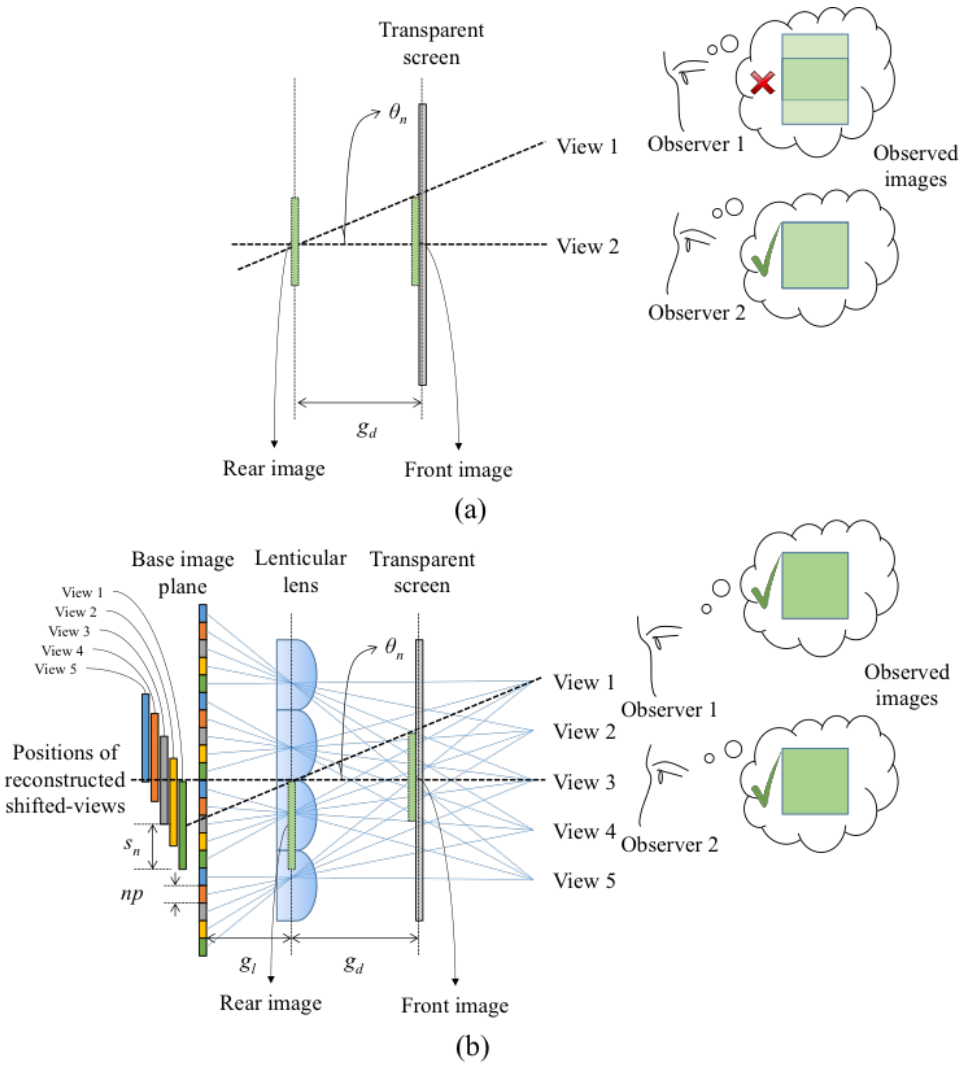

Figure 3.1 Comparison of the conventional DFD and viewing-angle-enhanced DFD: (a) Conventional DFD showing separated images for the side view, (b) DFD with multiple viewing points showing correct depth-fused image at the side view

shifted images are generated and interwoven as in a conventional multi-view display. The amount of shift s_n is decided by the gap of the DFD system, g_d, and tangent of viewing angle θ as shown in Eq. (3.1).

$$s_n = g_d \tan \theta_n, \tag{3.1}$$

$$\theta_n = \arctan \frac{(n-1)np}{g_l}, \tag{3.2}$$

where the viewing angle is given by Eq. (3.2), and the subscript n denotes n-th view point from the central view. np represents the pitch of one view of the base image for a multi-view system, and g_l is the gap between the base image and the lenticular lens. It is identical to the arctangent of view-interval over viewing distance. The number of views is an important factor deciding the quality of the reconstructed images. While large number of views can provide smoother transition between the views, the resolution of the image will be deteriorated with the increase of the number of views, and vice versa. The maximum shift is limited by the viewing angle of lenticular lens. In a multi-view display the viewing angle is decided by the specification of lenticular sheet [57, 58].

3.2.2 Depth enhancement using integral imaging

Similar to the enhancement of viewing angles, if the lens array is inserted, the rear part of the system works as if it is an integral imaging system. An integral imaging system is composed of a lenslet array and an elemental image. A lens array is composed of square-shaped lenslets which look like an eye of a fly, and an elemental image is a set of small images, each of which corresponds to each lenslet of the lens array. If an elemental image is observed through a lens array, a 3D image is reconstructed according to the configuration of the system [59]. Because an integral imaging system can represent a plane at the specific depth position, the rear plane can be optically translated to the farther position in order to increase the gap of a DFD system. The conceptual diagram of the system in comparison with a conventional system is shown in Fig. 3.2. The integral imaging can work in the virtual mode showing virtual images located behind the lens array. With virtual mode, the depth range of the system d can be increased without changing the volume of the system d_s as illustrated in Fig. 3.2(b). In Fig. 3.2(b) the total depth of the system is much smaller than the expressible depth range of the system, while the conventional system has the same depth range with the dimension of the system as shown in Fig. 3.2(a). The extended position d of the virtual plane is calculated according to Eq. (3.3) derived from the simple lens law.

$$d = \frac{g_i f}{g_i - f}, \tag{3.3}$$

where f is the focal length of the lenslet and g_i is the gap between lens array and elemental imaging plane. By replacing the rear image of the DFD system with integral imaging system, the depth range of the system can be expanded to the amount of d.

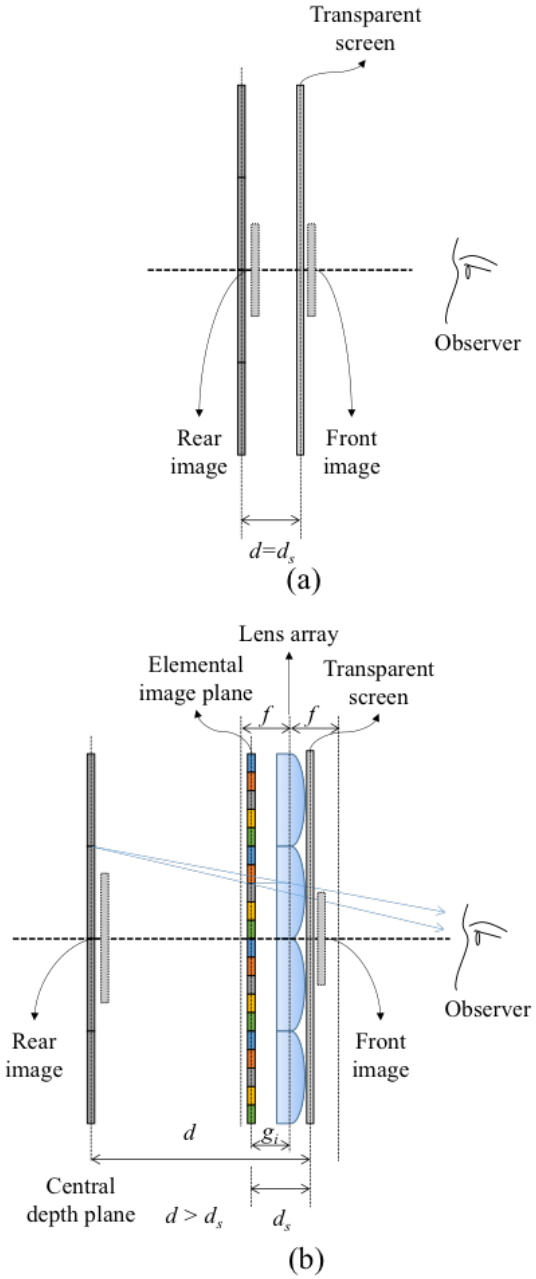

Figure 3.2 Comparison of the conventional DFD and depth-enhanced DFD. (a) Conventional DFD and (b) DFD with increased depth range with the same thickness of the display system

3.2.3 Depth and viewing angle enhancement

Although the concepts of the increasing viewing angle and depth are explained separately, both characteristics can be increased at the same time because of the similarity of the multi-view system and the integral imaging system as shown in the work of Wu *et al.* [60]. In the integral imaging system the viewer observes the magnified set of elemental images, meaning that the small portion of the elemental image set is actually shown at a specific viewing condition. The remaining area can be used for shifted views as in a one-dimensional integral imaging system using a lenticular lens which is very similar to a multi-view display. If the unused area is replaced with the shifted rear images, the system can increase the viewing angle as well as the depth range.

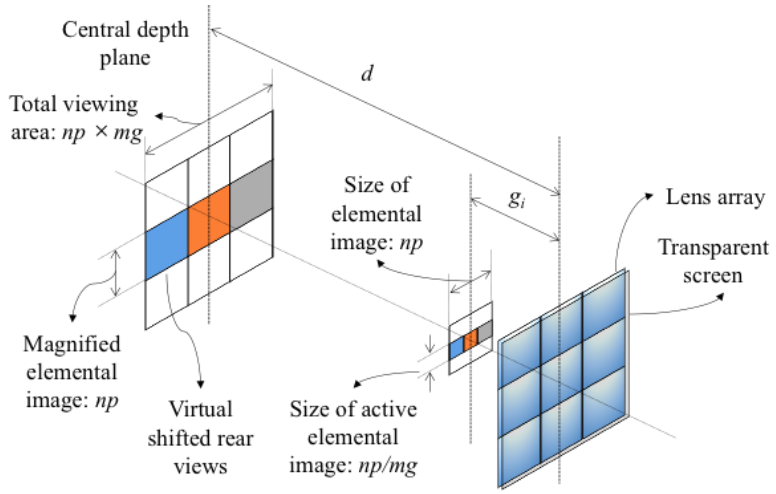

Figure 3.3 Relationship of the parameters of system components

In order to give a correct depth fusion, the sizes of the front and rear image should be matched considering the specifications of the optical components. The most important factor is the magnification of the lenslet. According to the

magnification, other parameters such as resolution, viewing angle and depth ranges are decided. The magnification is defined by the ratio of d to g_i, which is the distance from the lens array to the virtual imaging plane divided by the gap between the lens array and the elemental image. As shown in Fig. 3.3, the active area of the elemental image is reduced by the magnification factor mg, and the remaining area can be filled with shifted view images. The depth range of the system is increased by the magnification factor compared to the gap between the lens array and the elemental image. The maximum viewing angle is defined with regard to the case in which the viewer observes the outermost view of the elemental image, and the normal viewing angle is the angle of viewing direction from the central view. The viewing characteristics enhanced by lens array are summarized in Table 3.1. The viewing angles of additional views and the increase of number of views according to the magnification of a system are described in Fig. 3.4. The subscript in viewing angle in Table 3.1 denotes that the sequence of the viewing angle from the central viewing point and its maximum value can have half of the number of views nv. The increased number of views also reduces the crosstalk during the transition between the viewing positions. The crosstalk arises when the viewing position is changed to another position, but the dense viewing positions can provide the smoother transitions as in the conventional multi-view system. However, the increased number of view requires higher magnification factor as shown in Fig. 3.4, which aggravates the resolution of the image.

The author should also remark that the viewing angles and depth ranges increase at the same time with some restrictions. Because both parameters are highly dependent on each other, only optimal sets of the viewing angle and the depth range are provided. While the conventional DFDs are relatively free to adjust the depth range by changing the gap, the proposed system should have

Table 3.1 Parameters and their relationship of the viewing characteristics and system component

Category	*Parameters*	*Characteristics*
Viewing characteristics	Viewing angle	$\theta_n = \arctan \frac{n \cdot np}{g_i}$ for odd nv $\theta_n = \arctan \frac{(2n-1) \cdot np}{2g_i}$ for even nv
	Depth range	$d = g_i \cdot mg$
System parameters	Magnification	$mg = \frac{d}{g_i}$
	Number of views	$nv \leq \lfloor mg \rfloor$
	Size of image	$\frac{np}{mg}$

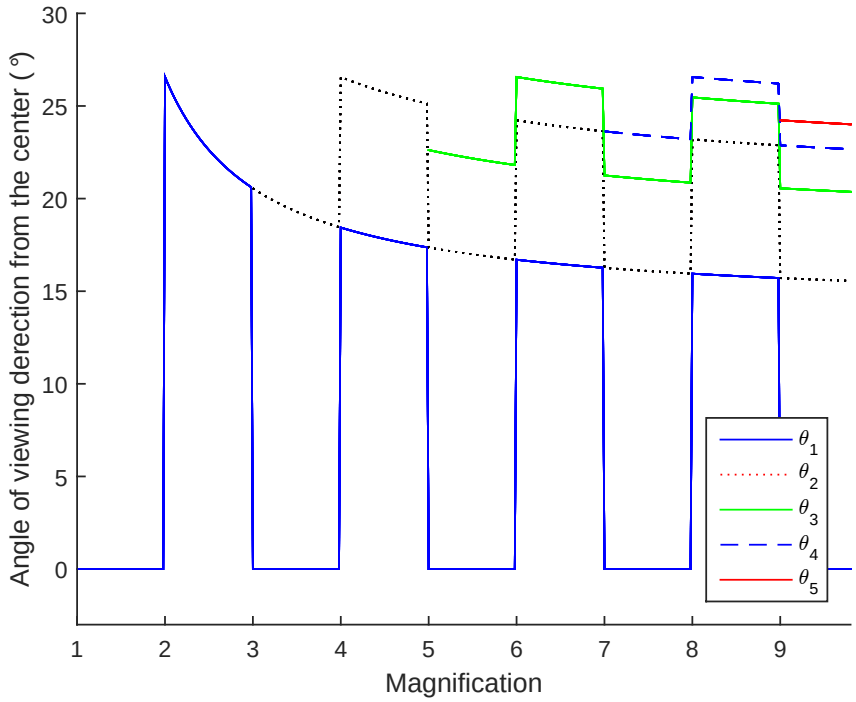

Figure 3.4 Angle of viewing direction from the center to each viewing point according to the magnification of the rear integral imaging system with parameters in Table 3.1

optimal depth decided by the multiplication of the magnification mg and the gap g_i of the integral imaging system in order to provide the correct depth-fusing effect. The resolution of the rear image is decreased by the magnification factor as well. For reducing the degradation of resolution, a small-pixel-pitched display can be adopted for a rear display. By applying proper image processing, the sizes of the front and rear images can be matched to provide a correct depth-fused image. Table 3.2 shows the comparison of viewing characteristics of the integral imaging, the proposed method, and the DFD method. Because the proposed method converts the resolution to the enhanced viewing angle and the resolution, the resolution of the system is relatively degraded compared to the conventional DFD method, but the depth range and viewing angle can be improved. While the integral imaging method provides modest depth range around the central depth plane according to the characteristic equation, the proposed method can provide larger depth range using the depth-fusing effect.

For achieving higher quality images, higher resolution of imaging system is required. As the resolution is reduced proportional to number of views, which is decided by the magnification factor as shown in Table 3.1, the number of pixel is reduced by $1/nv^2$. However, larger magnification increases the depth range of the system without physical expansion of the system. Conventional systems usually have expressible depth range between display panels, which is indicated as g_i in Fig. 3.3 while the proposed system have extended depth range by the amount of magnification factor, mg, as shown and illustrated in Table 3.1 and Fig. 3.3. By adjusting the parameters in Table 3.1, a proper balance of the resolution, the viewing angle and the depth range suitable for a specific application can be decided.

Typically, the depth range of the focused-mode integral imaging system is defined by the number of pixels allocated in the elemental images N multiplied

Table 3.2 Comparison of the integral imaging, depth-fused display, and the proposed method

	Integral imaging	*Depth-fused display*	*Proposed method*
Resolution	low	high	modest
Depth range	modest	low	high
Viewing angle	modest	very low	modest

by the focal length f of the elemental lens, which is given by Nf. For increasing the depth range, the number of pixels per elemental lens or focal length of the system should be increased. Current display technologies provides pixel pitches in the order of 100 μm, which provides approximately 10 pixels per 1mm size elemental lens. Consequently, the total depth range of the system will be 30 mm for a elemental lens having 3 mm of focal length. However, the proposed DFD system can provide longer depth. Provided that the DFD system has a identical spatial resolution to the aforementioned integral imaging system, the magnification will be 10. However, unlike the integral imaging system, it can work in the virtual mode. It means that larger size of lens having longer focal length can be used for optically translating the depth ranges. If we employ 10 mm size elemental lens having 30 mm of focal length, the total depth range becomes 270 mm for the proposed system.

3.3 Implementation of experimental system with enhanced viewing parameters

In order to demonstrate the feasibility of the system, the author implemented experimental system using flat panel displays (FPDs) and a lens array. Two kinds of FPDs having different pixel pitches are used to fabricate the system. Because the rear image is magnified, the pixel density of the rear display should be higher than that of the front display by the amount of magnification in order to prevent the degradation of the image resolution. The magnification, the resolution, and the depth range of the system are decided according to the specifications of the components. The specifications of the system parameters are summarized in Table 3.3.

Table 3.3 Specification of the experimental setup

Device	*Parameters*	*Values*
Front display	Size	18.5 inches
	Resolution	1366 × 768
	Pixel pitch	299.9 μm
Rear display	Size	5 inches
	Resolution	1920 × 1808
	Pixel pitch	57.5 μm
Elemental lens	Configuration	15 × 15
	Size	5 mm × 5 mm
	Focal length	10 mm
Front image	Resolution	251 × 188
	Depth position	0 mm
Front image	Resolution	1304 × 1304
	Depth position	-33 mm (calculated)
Integral imaging display	Magnification	4.3
	Number of view	3 ×3
Depth-fused display	Depth range	33 mm (calculated)
	Resolution	251 × 188
	Thickness of the system	20 mm

A computer generated 3D object is used for a source image. The 2D image and its corresponding depth map is generated using graphic software. With the given depth map, the 2D image is separated into the front and the rear base images according to the linear luminance and depth weight [34]. Although the dioptric distance should be used in calculating the luminance modulation, a conventional distance is used for simplifying the calculation because the result is not severely altered when the viewing distance is far enough compared to the depth range of the system. If the depth range of the system becomes comparatively larger, however, the viewing distance should be fixed, and dioptric distance should be used for calculation of the luminance modulation. The calculated rear image is then converted into an elemental image, but for assigning the shifted rear view images, only active portions of the elemental image are recorded. The obtained images of front, rear and converted rear images are shown in Fig. 3.3.

The remaining area of the converted rear elemental image is filled with the shifted rear images in order to extend the viewing angle of the system. According to the given parameters of the system, the shifting distance is calculated and applied to the converted rear image horizontally and vertically as shown in Fig. 3.3(a). Side view images are colored for clarifying the shift of the view. Figure 3.3(b) shows the combined elemental image of the shifted images and Fig. 3.3(c) shows an elemental image without any coloring. The red boxes in Figs. 3.3(b) and 3.3(c) indicate the elemental image assigned to a lenslet, and it is composed of the shifted sub-elemental images as shown in the magnified image at the lower right corner.

The experimental system is shown in Fig. 3.3(a). The gap between the

[2]The object is modeled by Kuhn Industries and used under Creative Commons Attribution 3.0.

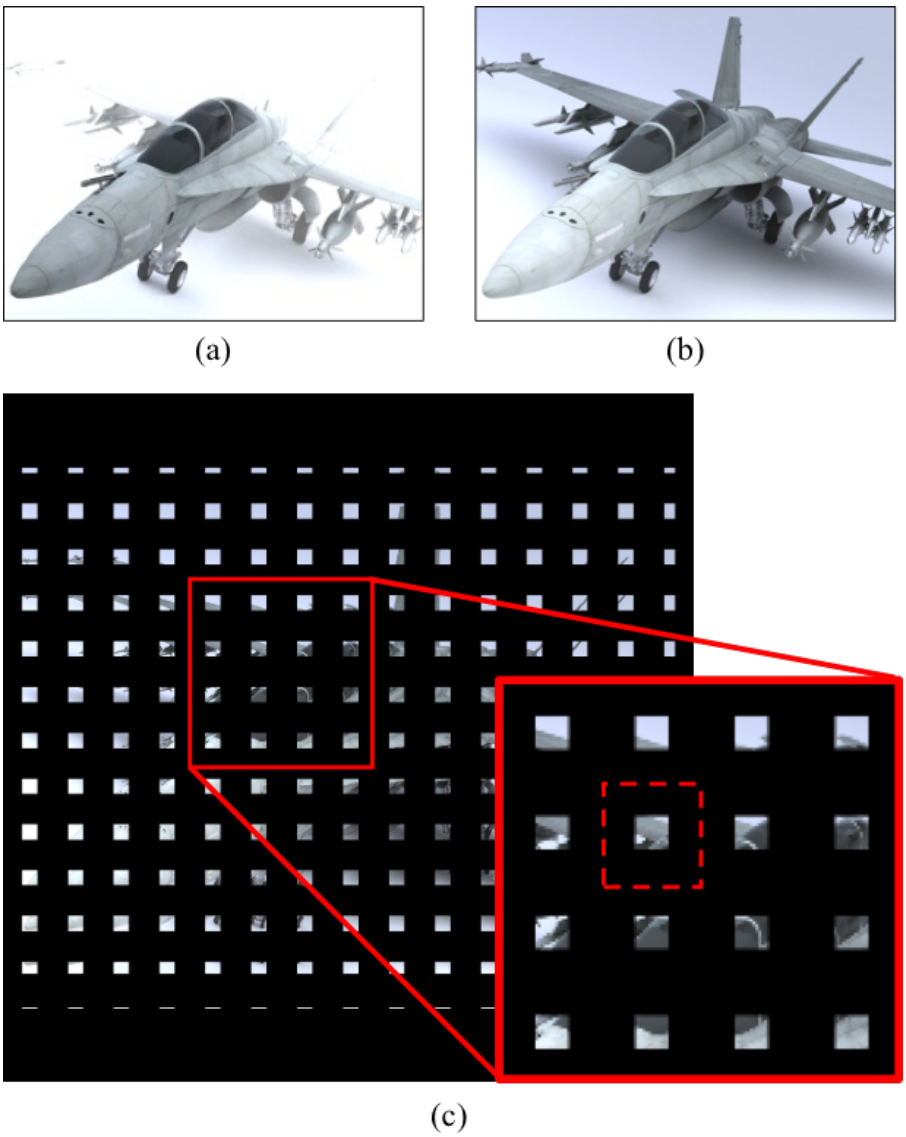

Figure 3.5 Source images[2]for the proposed DFD system: (a) front image, (b) rear image, and (c) converted rear image. The red box shows the enlarged elemental images, and the dashed square indicates the area of a lenslet of a lens array.

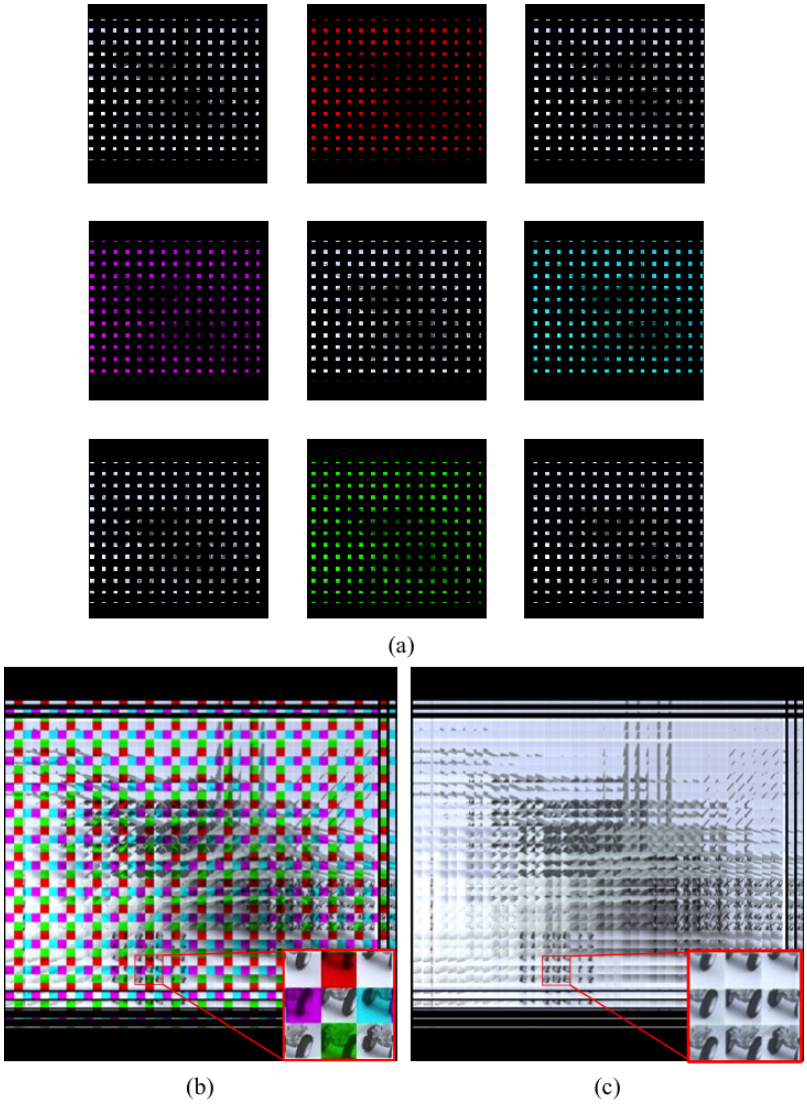

Figure 3.6 Elemental image set: (a) individual shifted rear images according to the viewing directions with differentiated color for the purpose of calibration, (b) combination of nine different elemental images shown in (a). The elemental image in the red box shows the combination of nine shifted-elemental images, and (c) combined elemental image. The red boxes show an elemental image allocated to a lenslet.

front display and rear lens array is about 7.7 mm, which gives virtual image at 33 mm behind the lens array although the total depth of the system is only 20 mm. Compared to the proposed method, the integral imaging system with the same experimental parameters can give 4 mm of depth range according to the characteristic equation [59], and the conventional DFD method with the same specifications can provide about 15 mm of depth range due to the system dimension.

Figure 3.8 shows additional viewing positions according to the viewing directions. Front and rear images are clearly fused when the viewer is located out of the central position. The expanded depth of the system can be confirmed using a half mirror as shown in Fig. 3.9. By combining the depth-fused image with the real target object as demonstrated in Fig. 3.9(c), the depth range of the system can be demonstrated. In the system the orange and the blue arrows indicate the optical path of depth-fused image and the target image respectively. In Fig. 3.9(a) the target is located at the head of the jet fighter while the target is located at the tale in Fig. 3.9(b). In both images, the target is

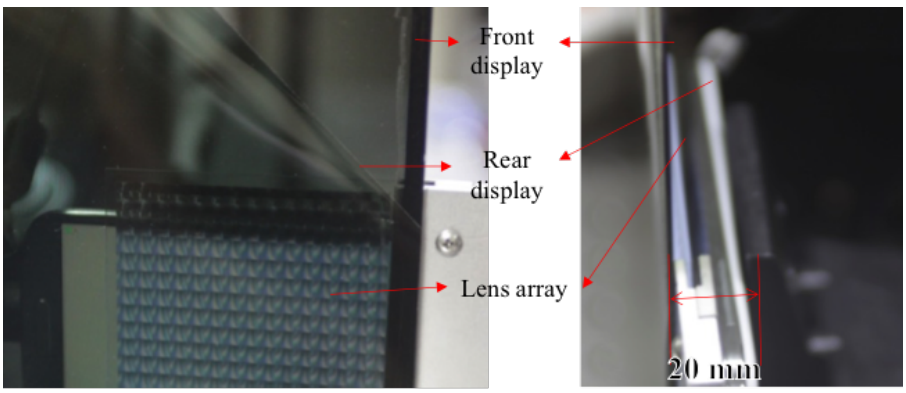

Figure 3.7 Experimental system: (a) front view of the experimental setup, (b) side view of the experimental setup. The total depth of the system is 20 mm.

clearly focused, and the gap between the two targets is 30 mm, which is slightly smaller than the calculated depth range (33 mm).

The moiré pattern that occurs due to the sub pixel structure of the rear display is shown through the lenslet array. In order to reduce the color moire, magnification should be reduced or horizontal sub-pixel structure can be adopted for reducing the horizontal color dispersion without compromising the magnification factor [61,62]. Recently, head-mounted display type depth-fused display has been proposed [63]. The system employs vari-focal lenses or mirrors modulating the focusing planes for achieving depth-fusing effect with a time-multiplexing method. However, the mechanical movement of the optical element entails the system complexity requiring precise alignment and synchronization between devices. In this viewpoint, the integral-imaging-based DFD approach can provide slimmer device size and simpler system configuration.

Also, brightness of the system is an important issue. As the LCD requires polarizer for modulating the intensity, the light efficiency of the system using a transparent LCD is reduce by less than half. The driving circuits of pixels and the color filter of the LCD also lower the transmittance resulting in 3% - 5% of the total transmittance. If the transmittance of LCD is increased by adopting field sequential color or inserting micro transparent windows, the transparency can be increased, which can be more energy efficient with reduced power consumption proper to the mobile applications. However, the enhancement of the brightness of the system requires development of the novel hardware devices, which is beyond the scope of the author's research. For achieving brighter images, the author used the maximum brightness of the LCDs for the experimental systems.

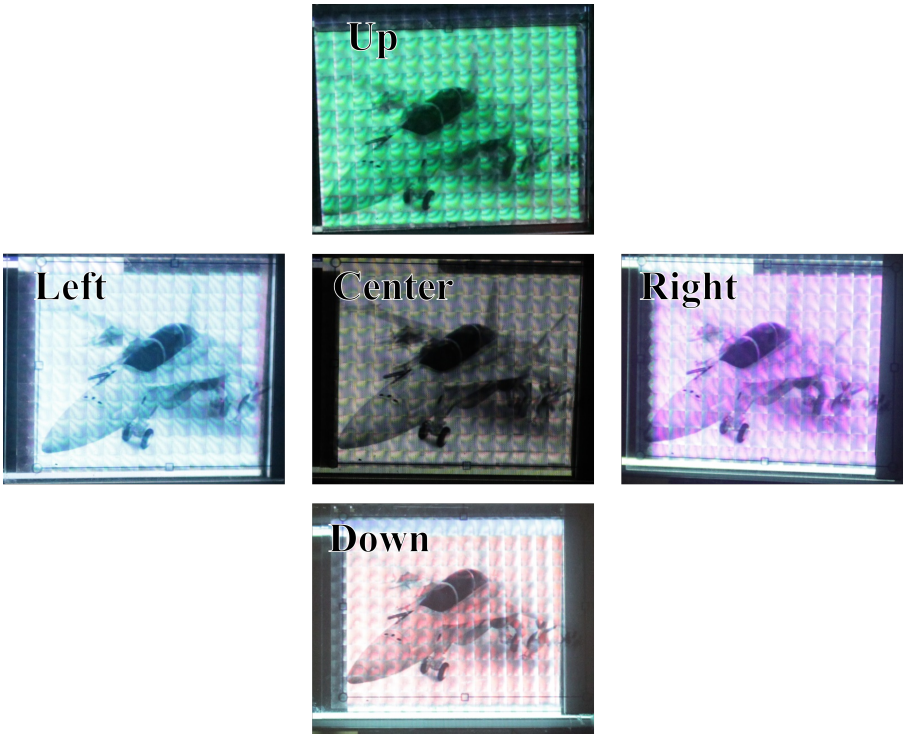

Figure 3.8 Result of the experimental system according to the different viewing angles

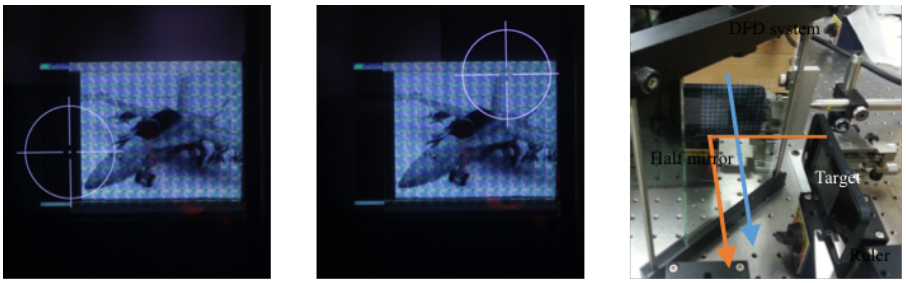

Figure 3.9 Comparison of the depth range of the proposed system using half mirror: (a) target located at the front image plane, (b) target located at the rear plane, and (c) half-mirror setup for finding depth range.

3.4 Summary

In this chapter, the author proposed a DFD system which can be seen at wider viewing angles with extended depth range. The author expects that the proposed system has advantages in viewing conditions as well as the quality of the reconstructed 3D images compared to other 3D display methods. Another advantage of the proposed system is its compactness. Although other volumetric displays require bulky volumes to represent voxels, the proposed system can generate voxels within a virtual space. Based on the analysis of the system parameters, proper adjustment of each viewing parameter would widen the range of applications for the DFD with specific purposes such as a personal portable 3D display with large depth range or a wide viewing angle display for multiple viewers.

Chapter 4

Real-mode depth-fused display with viewer tracking

4.1 Introduction

3D displays have been considered as next generation displays for a long time. Although autostereoscopic 3D displays have been studied more than hundred years, realization of a high-quality 3D image as good as objects in real world is still hard to achieve [1]. The reason is that required amount of information is too burdensome to achieve with current technologies. Moreover, the trade-off between the viewing parameters also hinders the realization of the natural and high-quality 3D system [59, 64]. As mentioned in the introduction of this dissertation, it is well known that four physiological factors of depth perception are essential for achieving natural 3D experience, which are binocular disparity, convergence, accommodation and motion parallax. Binocular disparity and convergence are easily implemented in conventional 3D display systems due to the moderated requirement of resources, which requires only two different view

images. However, the other factors are hard to be reached because the required amount of the information is multiplicative along with the number of views. Based on the ray optics or directional view approaches, at least two different view images should be superimposed on one eye in order to induce accommodation response satisfying super multi-view condition [22]. For realizing the super multi-view condition, very dense bundle of rays should be provided. In the previous studies, it was usually achieved by employing multiple display devices or high resolution displays [27–29, 65–67]. Recently, some of pioneering work proposed that compressive optimization of the view images can greatly reduce the system complexity [14, 15]. However, the compressive display methods require high speed displays for achieving temporal multiplexing of the system. They are promising technology, but further development of the display technology such as transparency or driving speed is required for realizing commercial quality of the system. Moreover, view-image based accommodation is highly dependent on the observer's viewing distance because the density of view image decreased as the observer becomes distant from the display. For this reason, those systems have limited viewing distance where satisfying the super multi-view condition. Depth-fused displays (DFDs), however, provide accommodation cue with a different approach. They exploit physiological characteristics of the human eye to provide accommodation. When the viewer observes depth-fused 3D images, the focusing position is adjusted to give the maximum contrast of the retinal image, which is the combination of overlapped plane images [32–34]. It is also reported that the difference at the edge of the overlapped image gives binocular disparity which results in the perception of depth change according to the luminance ratio [31, 51]. Consequently, the accommodation property of the DFD system is maintained regardless of the viewer's distance from the display as the luminance ratio of the front and rear image is the only factor that affects

the accommodation, and it is not altered by the viewing distance. By using this volumetric property of the depth-fused display, the viewing condition can be greatly improved combined with the tracking technology. In this chapter, further developed DFD system is presented by employing a viewer tracking method in addition to the combination with an integral imaging method [68]. Similar to the previous method, combination of DFD with an integral imaging system can increase the depth range and viewing angle at the same time. In this configuration, the integral imaging system only shows a plane image, which is just floated from the display plane to the new position. With the real-mode integral imaging setup, the floated image can be located in front of the lens array, and it can give depth-fusing effect with the rear image being displayed on the transparent display screen, which is located on the lens array. As a result, 3D image can be generated in mid-air in front of the display, which is very hard to achieve with the conventional DFDs. Also, the tracking enables the dynamic parallax and widening of viewing angle. For showing the feasibility of the proposed method, the author conducted an experiment demonstrating the improved viewing conditions compared to the conventional integral imaging and DFD systems.

4.2 Viewer tracking method

The proposed system is composed of two parts as shown in Fig. 4.1. One is the viewer-tracked integral imaging system, and the other is the viewer-tracked DFD. The viewer-tracked integral imaging system is based on the previous studies, but the difference is that the proposed system reconstructs only a 2D plane image instead of providing a 3D image because 3D effect is given by the depth-fusing effect. In addition, the viewing angle of the system is also kept as small as possible, which covers both eyes of the observer as the viewing angle can be extended with the tracking method, which results in minimization of resolution loss. Also, motion parallax does not need to be provided in the integral imaging system because dynamic parallax is provided with the tracking system. Consequently, the spatial resolution of the reconstructed image can be relatively less degraded compared to the conventional integral imaging system which gives similar depth range and viewing angle.

4.2.1 Viewer-tracked depth-fused display

The viewing angle of DFD can be defined as the maximum angular span where the viewer observes a correct overlapped image. However, in a conventional DFD system, the viewing angle is extremely limited because even slight misalignment of the overlapped image breaks the depth-fusing condition. As a result, the DFD gives correct image only at the fixed viewing direction. Previous research proposed solution of the narrow viewing angle by adapting multi-view method for providing shifted view images along with the shifted position of the viewer [35, 68]. However, the provision of the extra viewing positions requires sacrifice of the spatial resolution of the image or additional display device for other viewpoints. We employed dynamic shifting of the image for solving this problem. It can be simply implemented by adopting viewer tracking system [36]. The

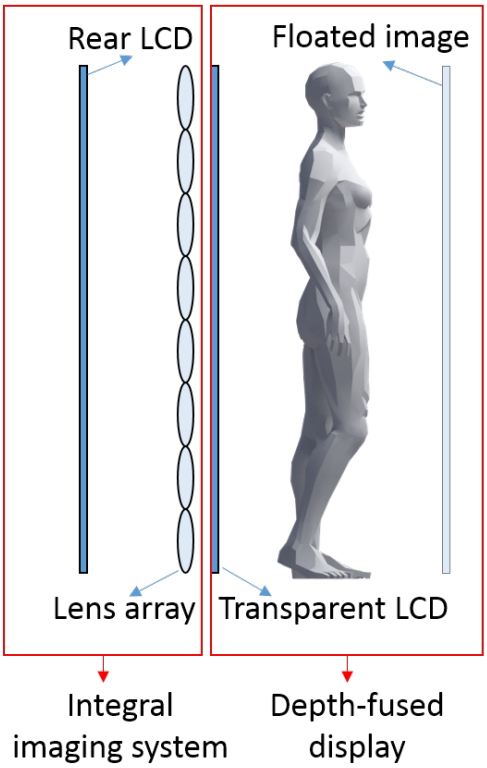

Figure 4.1 Configuration of the proposed system[1]

viewing direction of the observer can be obtained from the tracking sensor, and the image can be shifted to compensate the viewer's deviation angle from the center of the display as illustrated in Fig. 4.2.

In addition to the expansion of the viewing angle, the tracking method gives another benefit to the DFD system, which is the motion parallax. While the previous study proposed a DFD system with multiple viewing zones, the system could not give the parallax of the object. That means, although the viewer changes the position, the parallax of the observed image is not changed as in the glasses-type stereoscopic 3D images. However, by updating the source

[1]The human figure shown in the figure is provided by Alexander Lee, and it is used under Creative Commons Attribution 3.0.

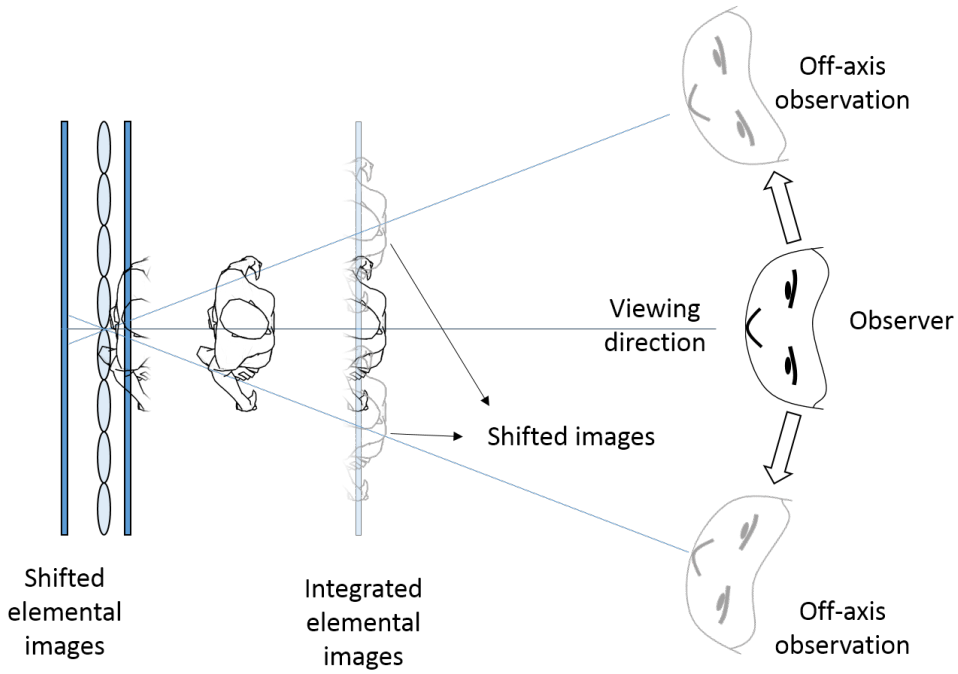

Figure 4.2 Concept of the compensation of viewer's off-axis position

image according to the corresponding parallax images, motion parallax can be provided through the system. These kinds of tracking method is commonly used in the horizontal-parallax-only 3D systems to give vertical parallaxes [28, 45]. However, as a DFD system does not have any parallaxes in a stacked configuration, both horizontal and vertical parallax should be given with the tracking method. In order to provide parallaxes in a DFD system, view images having angular parallax are converted into base images for the system according to the obtained viewer's position from the tracking sensor.

4.2.2 Viewer-tracked integral imaging for a depth-fused display

It is reported that tracking is an effective method for achieving wider viewing angle in an integral imaging system [69, 70]. In the proposed method, a real-mode integral imaging system is used for displaying a front base image of a depth-fused 3D image. As mentioned earlier, the reconstructed image is a plane image, of which the viewing angle covers the viewer's both eyes. Because the viewing angle is extended by the tracking method, it does not need to be wider than the aforementioned condition, and it keeps the spatial resolution of the image as high as possible. Viewing angle of integral imaging indicates the maximum allowance of the viewer's position in angular displacement. It can be calculated from the geometry of the lens and the elemental image as shown in Fig. 4.3 and in Eqs. (4.1) and (4.2) [59]. Ω_c is the viewing direction; Ω_S is the span of viewing angle; g is the gap between lens array and elemental images; s is the shift amount of the elemental images; and p_l is the size of elemental image and elemental lens. As shown in the equation, the larger area of the elemental image results in a wider viewing angle. Or by declining the optical axis with shifted elemental images, the center of the viewing angle can be steered according to the tracked viewer's position, which is called adapted elemental

images [69, 70]. However, the angular span of the viewing angle is decreased as the declined angle becomes steeper. It can also be calculated from the geometry of the elemental image and elemental lens as shown in Eqs. (4.1) and (4.2) with the shifting parameter s.

$$\Omega_s = \arctan\left(\frac{s + p_l/2}{g}\right) - \arctan\left(\frac{s - p_l/2}{g}\right), \tag{4.1}$$

$$\Omega_c = \frac{1}{2}\left[\arctan\left(\frac{s + p_l/2}{g}\right) + \arctan\left(\frac{s - p_l/2}{g}\right)\right]. \tag{4.2}$$

Figure 4.4 shows the viewing angle of the example system with 10 mm lens array having focal length of 22 mm and 50 mm of central depth plane (CDP). As shown in the graph, the span of the viewing angle decreases as the deviation of the observer's viewing direction becomes steeper. The decreased viewing angle should cover the both eyes in order to prevent the cracking or flipping of the reconstructed images. The coverage viewing angle Ω_{cv} can be calculated as follows.

$$\Omega_{cv} = 2\arctan\frac{I_{PD}}{2D}, \tag{4.3}$$

where D stands for the viewing distance of the observer, and I_{PD} is the inter-pupil distance, which is usually 65 mm for adults. Usually, viewing distance in an integral imaging system with n elemental lenses is longer than minimum viewing distance D_m, which is given as $g\,(n-1)$. The coverage angle is maximized at the minimum viewing distance. As a result, if the maximum coverage viewing angle Ω_{cv} is greater than the span of the viewing angle Ω_s, a correct plane image is observed by the viewer as shown in Fig. 4.5.

Figure 3.3 shows the criteria which decides the viewing angle of the proposed system. As shown in the graph, smaller angle value between the viewing angle

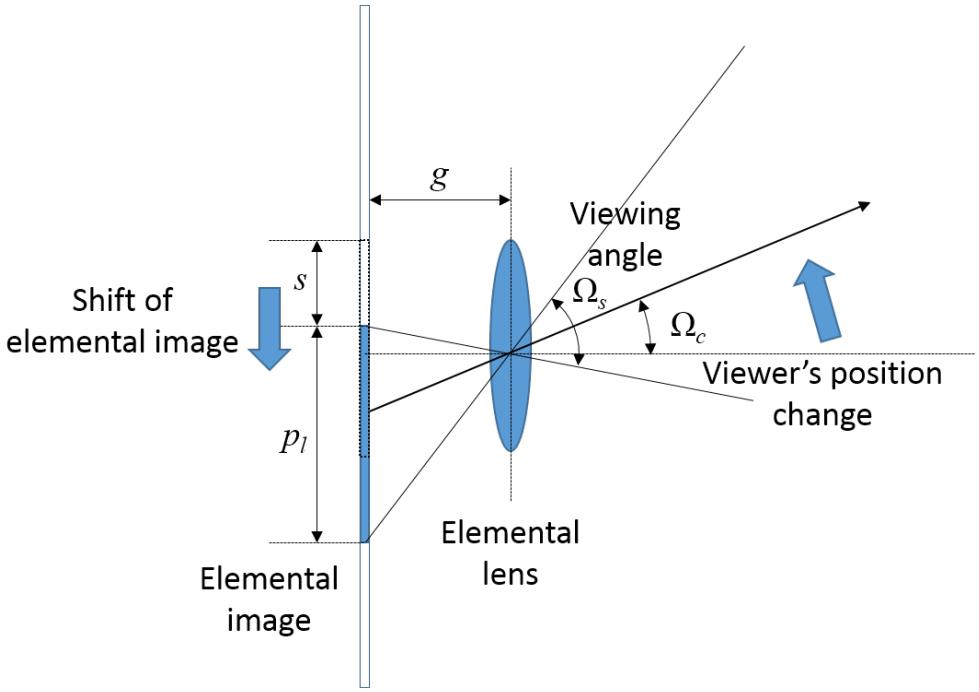

Figure 4.3 Geometry of the viewing angle for the shifted elemental image

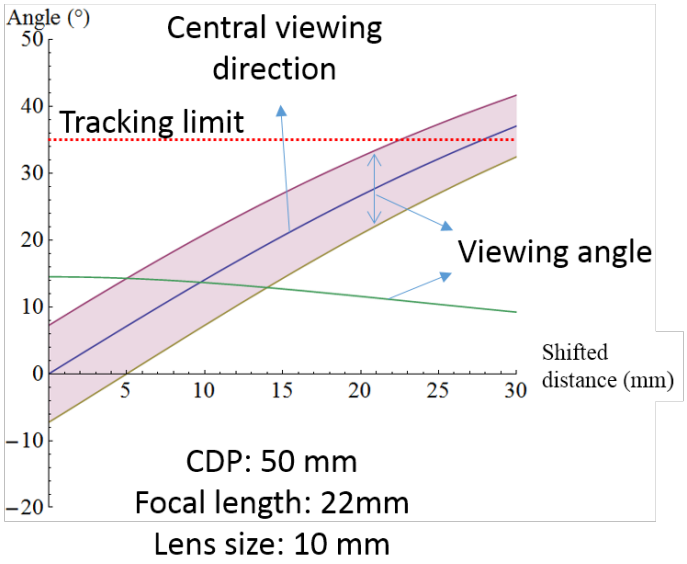

Figure 4.4 Span of the viewing angle according to the viewing direction

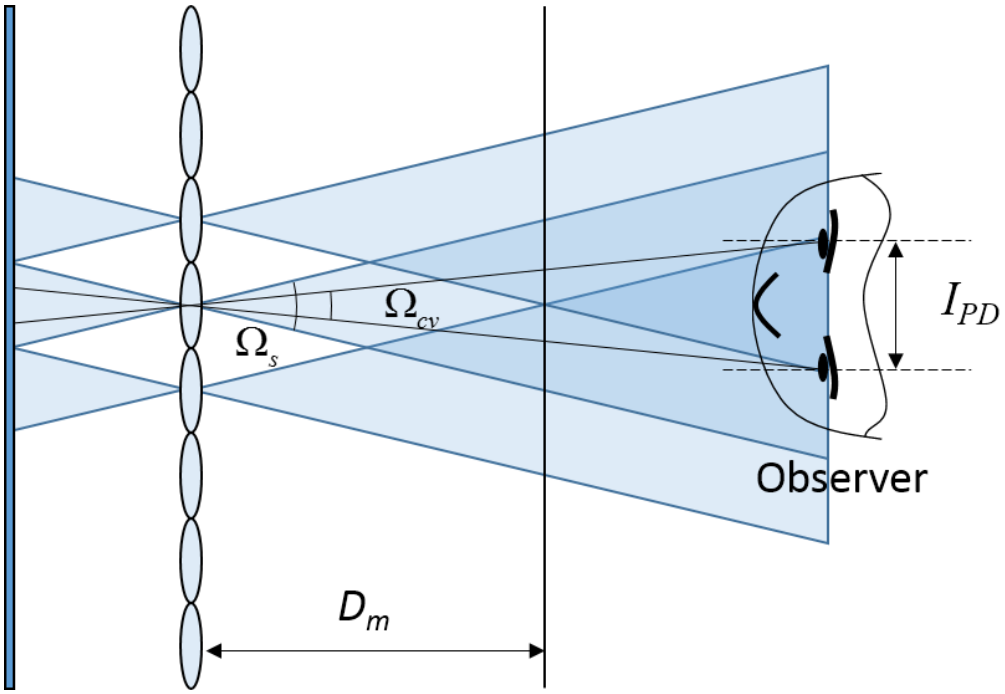

Figure 4.5 Coverage angle for binocular condition

decided by the coverage angle and the tracking limit of the sensor decides the viewing angle of the system. The example system shown in the graph is composed of 1 mm lens array with focal length of 3.3 mm, and the CDP of the system is 30 mm. Provided that the D_m is 500 mm, the maximum coverage angle becomes approximately 8°, and it results in 45° of maximum viewing angle for single direction, which gives total 90° of viewing angle. However, the tracking limit of the system is 35° resulting the narrowing of the effective viewing angle to 70°. According to the system parameters, viewing angle can be changed. The proper viewing angle should be found for specific applications in order to conserve the spatial resolution as high as possible. In extreme case, if the floating distance becomes the half of the focal length of the system, the resolution loss becomes zero as there is no magnification of the floated base image.

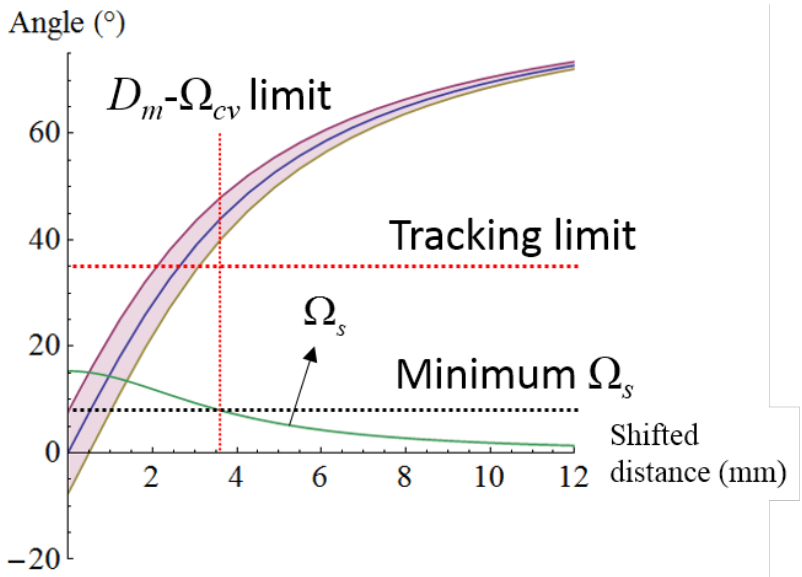

Figure 4.6 Criteria for viewing angle

4.3 Implementation of viewer-tracked integral imaging

For showing the feasibility of the proposed method, experimental system is implemented. The experimental system contains two liquid crystal displays (LCDs). One is for implementation of integral imaging system and the other is for depth-fusing effect. The LCD for depth-fusing effect is modified by eliminating the backlight unit and the rear polarization film so that it becomes transparent. Between the two LCDs, lens array is located as shown in Fig. 4.1. For the tracking sensor, an off-the-shelf webcam[2] is used, whose field-of-view is approximately 70° horizontally and 40° vertically. Blender[3] is used to generate parallax images with equiangular spacing. 60 views images for horizontal direction and 15 view images for vertical direction are captured resulting in total 900 view images within the field-of-view of the tracking sensor. For demonstrating the image preparation process, image processing procedure is illustrated in Fig. 4.7(a) with some of the sample view images. For each view image, corresponding depth information is saved for preparation of the depth-fused images. According to the linear depth weight, the view image is separated into front and rear base images as shown in Fig. 4.7(b).

Figure 4.8 shows the tracked observer's viewing direction and corresponding set of view images. In the experiment, the images are pre-processed, and the system only detects the viewer's position and shows the relevant view images according to the position.

Configuration of the experimental system is shown in Fig. 4.9. For the lens array, 13 by 13 square Fresnel lenses are used, of which the focal length is 22 mm with 10 mm of size. The gap between the front lens array and the

[2]C920, Logitech
[3]http://www.blender.org

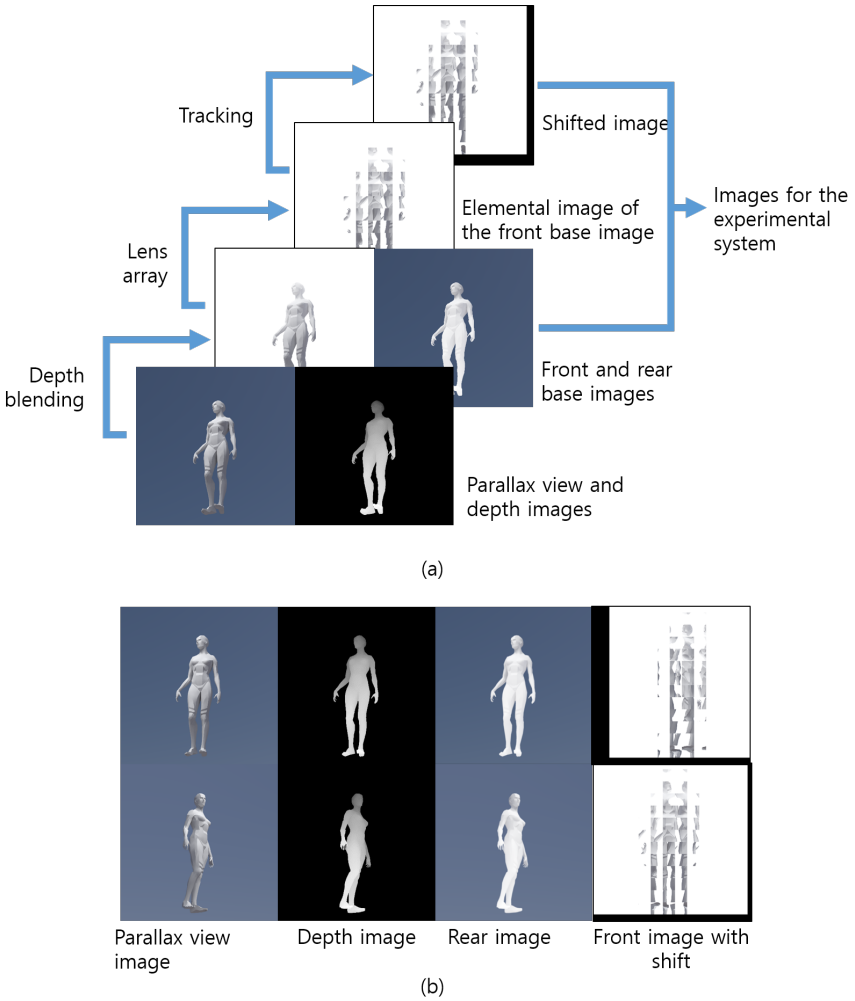

Figure 4.7 Preparation of source image: (a) procedure of image processing for the proposed system, (b) sample images for two different viewing directions

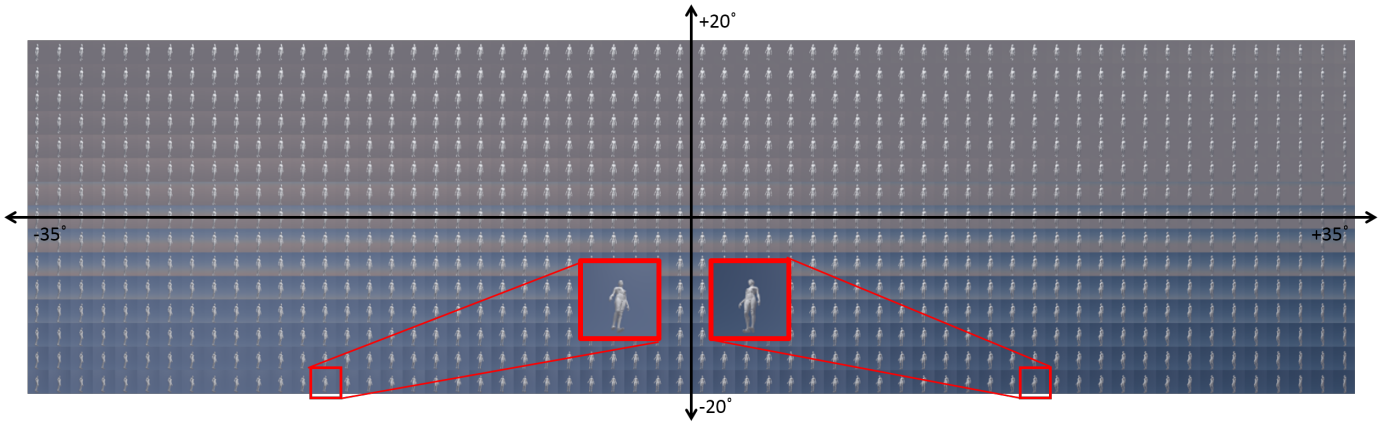

Figure 4.8 Perpective images of the experimental object

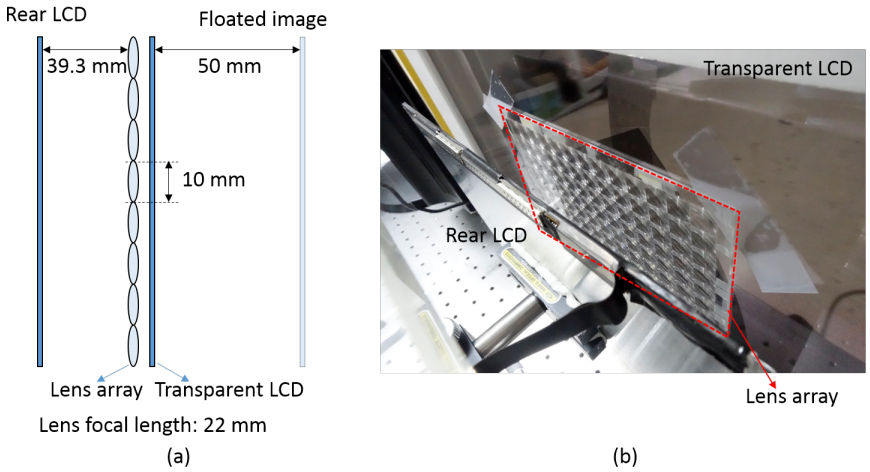

Figure 4.9 Configuration of the experimental setup: (a) schematic diagram of the experimental setup, (b) photograph of the experimental setup observed from the rear side

display is 39.3 mm, and the floated images are located 50 mm in front of the lens array. Figure 4.10 shows the front and rear base images generated by the experimental system. At the imaging positions for each base image, diffuser is located in order to verify the images themselves and their locations. As a result the depth range of the experimental system is 0 – 50 mm in front of the lens array. The innate viewing angle of the integral imaging system is 15° which is large enough to cover the both eyes, and the tracked viewing angle is increased by 70° horizontally and 40° vertically according to the tracking sensor. The specification of the experimental system is summarized in Table 4.1.

The experimental system in Fig. 4.11 shows the real-time tracking and response of view images. Because the camera is in a fixed location instead of the viewer's position, the front base image provided by integral imaging is cracked in the figure, but it is correctly reconstructed at the observer's position. As shown in the Fig. 4.12, corresponding set of base images shown by the DFD

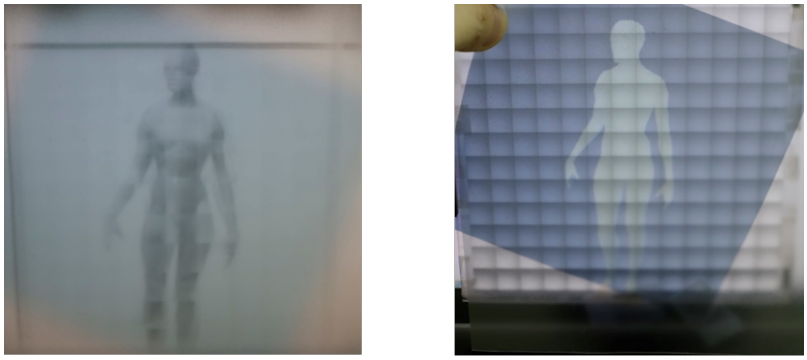

Figure 4.10 Resultant front and rear images generated by experimental system: (a) front image located 50 mm in front of the display and (b) rear image located on the rear display.

Table 4.1 Specifications of the experimental system

Parameters	*Values*
Viewing angle	70(h) × 40(v)
Resolution	494(h) × 494(v)
Image size	130 mm(h) × 130 mm(v)
Depth range	0 mm - 50 mm
Minimum viewing distance	510 mm form the display

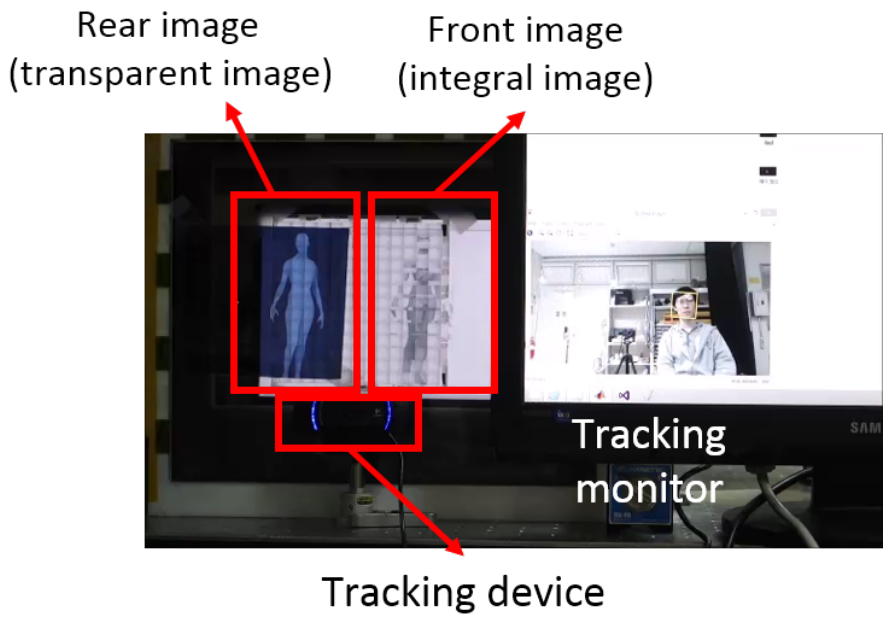

Figure 4.11 Tracking configuration of the observer and image response according to the tracked viewer's position. According to the detected viewer's position, front elemental image is shifted as well as the parallax.

system according to the obtained viewing direction of the observer is correctly superimposed resulting in a depth-fused 3D image with motion parallax.

In order to achieve larger depth range, the viewing perspective of human eye should be considered because the overlapped area for front and rear image changes according to the viewing distance. By using a depth sensor such as Kinect[4], precise viewing position of the observer can be obtained, and it can be used to calculate the perspective of the observer. Also, a lens array with longer focal length can be used in the system for increasing the floating distance, but the longer focal length results in the narrowing of the viewing angle due to the larger f-number. Although tracking method is used, the minimum viewing angle of the system should be larger than the coverage angle of both eyes as mentioned in the previous section. Additional motion sensors may enable the interactive function of the system like previous systems [71, 72]. As the reconstructed images are placed in front of the screen, users can freely interact with the reconstructed 3D object. Combined with a textile feedback [73], it will be applied in more applications such as demonstration of industrial design, medical imaging for surgical planning, or education.

For more realistic interactive applications, the characteristics of the display are also important. For example, small latency of the sensor and fast response time of the display are essential for dynamic interactive applications. In this kind of system, the flat panel displays having fast response time such as OLED display can be used, combined with fast motion sensors. Also, in order to keep the system volume small and compact, motion sensors should be integrated into the display setup.

[4]https://www.microsoft.com/en-us/kinectforwindows/

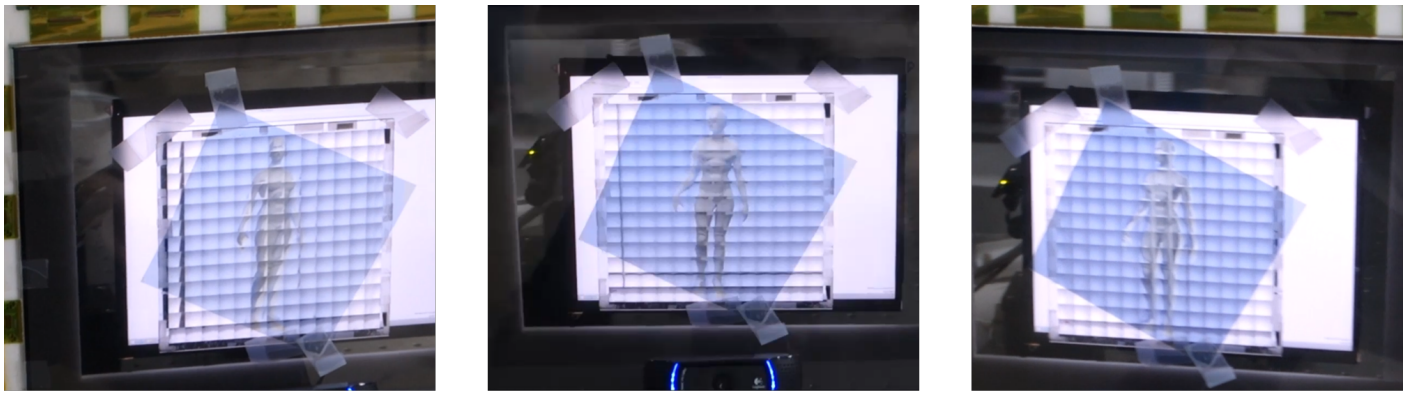

Figure 4.12 Experimental result of the proposed system at the viewer's position. Change of the parallax is shown within the viewing zone.

4.4 Summary

In this chapter, real-mode depth-fused display is proposed by employing integral imaging method and viewer tracking system. By generating 3D image with depth-fusion and viewer tracking method, viewing condition of the system is greatly improved for a single tracked user. With the depth-fusing effect and its volumetric characteristics, the proposed system can provide most of the major 3D depth cues, including accommodation, and motion parallax in a very wide range of viewing zone. In addition, the volume of the system is as thin as conventional flat panel displays, while the expressible depth range of the system is greater than its physical volume due to the characteristics of integral imaging system. If the lens array with shorter focal length is adopted, the current gap between the lens array and rear LCD can be more reduced. The author believes that the proposed method is a promising technology for personal 3D applications such as cell phones, media players.

Chapter 5

Conclusion

The volumetric characteristic of the depth-fused display enables great improvement of the accommodation characteristic of the 3D displays while the light field displays including multi-view displays, integral imaging displays, and even super multi-view displays have limited provision of accommodation cues. The accommodation in those systems is highly dependent on the ray density which is gradually decreased as it propagates from the screen. As a results, the viewing area that provides all of the physiological depth cues is restricted to the adjacent of the display screen. Depth-fused displays do not suffer from those problems related to the viewing distance as the plane images are correctly positioned on the visual axis of the observer, but if the observer's position is changed, the images are observed as separated two plane images. It was serious drawback of the depth-fused displays, as it limits even slight movement of observer. In this dissertation, various methods overcoming the drawback of limited viewing characteristics are proposed by employing projection system or 3D display methods. Depth-fused displays combined with projection-type displays can have multiple

layers of depth-sectioned images which can give more volumetric characteristics of the system. Also, by adopting polarization-encoded depth information techniques, the proposed system can have simple configuration as conventional projection-type displays. As 3D images are generated from the depth and 2D color images, the proposed system shows high compatibility with off-the-shelf depth-cameras, which are expected to be integrated in many mobile devices[1]. If these technologies are popularized, 3D image contents will be easily obtained by non-expert users. Combination of depth-fused display with multi-view or integral imaging display will find promising mobile or personal 3D applications. As the volume of the system can be kept as thin as conventional flat-panel mobile displays while the provided depth range is thicker than that of conventional multi-view or integral imaging displays. In addition to the enhanced depth range, the volumetric characteristics of the system will provide very natural 3D images by satisfying binocular disparity, convergence, accommodation, and motion parallax. Future research may contain the interactive application of the proposed method by adopting depth camera or other depth capturing devices. Or motion sensing devices can result in a interactive applications with the reconstructed 3D images.

[1]Intel Real Sense, http://www.intel.com/content/www/us/en/architecture-and-technology/realsense-overview.html

Bibliography

[1] B. Lee, "Three-dimensional displays, past and present," Phys. Today **66**, 36–41 (2013).

[2] E. B. Goldstein, *Sensation and Perception* (Cengage Learning, 2013), 9th ed.

[3] F. A. Miles, S. J. Judge, and L. M. Optican, "Optically induced changes in the couplings between vergence and accommodation." J. Neurosci. **7**, 2576–2589 (1987).

[4] D. M. Hoffman, A. R. Girshick, K. Akeley, and M. S. Banks, "Vergence–accommodation conflicts hinder visual performance and cause visual fatigue," J. Vis. **8**, 33–33 (2008).

[5] S. Nagata, "How to reinforce perception of depth in single two-dimensional pictures," in "Pictorial communication in virtual and real environments," R. E. Stephen, ed. (Taylor & Francis, Inc., 1991), pp. 527–545.

[6] J. Geng, "Three-dimensional display technologies," Adv. Opt. Photon. **5**, 456–535 (2013).

[7] Oculus, "http://www.oculus.com," (2013).

[8] A. Maimone, D. Lanman, K. Rathinavel, K. Keller, D. Luebke, and H. Fuchs, "Pinlight displays," ACM Transactions on Graphics (TOG) **33**, 89 (2014).

[9] Y. Kim, J. Kim, J.-M. Kang, J.-H. Jung, H. Choi, and B. Lee, "Point light source integral imaging with improved resolution and viewing angle by the use of electrically movable pinhole array," Opt. Express **15**, 18253–18267 (2007).

[10] T. Peterka, R. L. Kooima, D. J. Sandin, A. Johnson, J. Leigh, and T. A. DeFanti, "Advances in the dynallax solid-state dynamic parallax barrier autostereoscopic visualization display system," IEEE Transactions on Visualization and Computer Graphics **14**, 487–499 (2008).

[11] M. Levoy and P. Hanrahan, "Light field rendering," in SIGGRAPH '96, (ACM Request Permissions, New York, New York, USA, 1996), pp. 31–42.

[12] H. Gotoda, "A multilayer liquid crystal display for autostereoscopic 3D viewing," Proc. SPIE **7524**, 75240P–75240P–8 (2010).

[13] D. Lanman, M. Hirsch, Y. Kim, and R. Raskar, "Content-adaptive parallax barriers: optimizing dual-layer 3D displays using low-rank light field factorization," ACM Transactions on Graphics (TOG) **29**, 163 (2010).

[14] G. Wetzstein, D. Lanman, M. Hirsch, and R. Raskar, "Tensor displays: compressive light field synthesis using multilayer displays with directional backlighting," ACM Transactions on Graphics (TOG) **31**, 1–11 (2012).

[15] M. Hirsch, G. Wetzstein, and R. Raskar, "A compressive light field projection system," ACM Transactions on Graphics (TOG) **33**, 58–12 (2014).

[16] G. E. Favalora, J. Napoli, D. M. Hall, R. K. Dorval, M. Giovinco, M. J. Richmond, and W. S. Chun, "100-million-voxel volumetric display," Proc. SPIE **4712**, 300–312 (2002).

[17] A. Sullivan, "DepthCube solid-state 3D volumetric display," Proc. SPIE **5291**, 279–284 (2004).

[18] H. Kimura, T. Uchiyama, and H. Yoshikawa, "Laser produced 3D display in the air," in SIGGRAPH '06, (ACM Press, Boston, MA, USA, 2006), p. 20.

[19] P. A. Blanche, A. Bablumian, R. Voorakaranam, C. Christenson, W. Lin, T. Gu, D. Flores, P. Wang, W. Y. Hsieh, M. Kathaperumal, B. Rachwal, O. Siddiqui, J. Thomas, R. A. Norwood, M. Yamamoto, and N. Peyghambarian, "Holographic three-dimensional telepresence using large-area photorefractive polymer," Nature **468**, 80–83 (2010).

[20] J. Hahn, H. Kim, Y. Lim, G. Park, and B. Lee, "Wide viewing angle dynamic holographic stereogram with a curved array of spatial light modulators," Opt. Express **16**, 12372–12386 (2008).

[21] A. Maimone, G. Wetzstein, M. Hirsch, D. Lanman, R. Raskar, and H. Fuchs, "Focus 3D: Compressive accommodation display," ACM Transactions on Graphics (TOG) **32** (2013).

[22] Y. Kajiki, H. Yoshikawa, and T. Honda, "Hologram-like video images by 45-view stereoscopic display," Proc. SPIE **3012**, 154–166 (1997).

[23] Y. T. N. Nago, "Multi-projection of lenticular displays to construct a 256-view super multi-view display," Opt. Express **18**, 8824–8835 (2010).

[24] Y. Takaki, K. Tanaka, and J. Nakamura, "Super multi-view display with a lower resolution flat-panel display," Opt. Express **19**, 4129–4139 (2011).

[25] Y. Takaki, Y. Urano, S. Kashiwada, H. Ando, and K. Nakamura, "Super multi-view windshield display for long-distance image information presentation," Opt. Express **19**, 704–716 (2011).

[26] J. Nakamura, K. Tanaka, and Y. Takaki, "Increase in depth of field of eyes using reduced-view super multi-view displays," Appl. Phys. Express **6**, 022501 (2013).

[27] J.-H. Lee, J. Park, D. Nam, S. Y. Choi, D.-S. Park, and C. Y. Kim, "Optimal projector configuration design for 300-Mpixel multi-projection 3D display," Opt. Express **21**, 26820–26835 (2013).

[28] A. Jones, K. Nagano, J. Liu, J. Busch, X. Yu, M. Bolas, and P. Debevec, "Interpolating vertical parallax for an autostereoscopic three-dimensional projector array," J. Electron. Imaging **23**, 011005 (2014).

[29] A. Jones, J. Unger, K. Nagano, J. Busch, X. Yu, H.-Y. Peng, O. Alexander, and P. Debevec, "Creating a life-sized automultiscopic Morgan Spurlock for CNNs 'Inside Man'," in SIGGRAPH '14, (ACM Press, New York, New York, USA, 2014), pp. 1–1.

[30] S. Katz, A. Tal, and R. Basri, "Direct visibility of point sets," ACM Transactions on Graphics (TOG) **26**, 24 (2007).

[31] S. Suyama, S. Ohtsuka, H. Takada, K. Uehira, and S. Sakai, "Apparent 3-D image perceived from luminance-modulated two 2-D images displayed at different depths," Vision Research **44**, 785–793 (2004).

[32] K. Akeley, S. J. Watt, A. R. Girshick, and M. S. Banks, "A stereo display prototype with multiple focal distances," ACM Transactions on Graphics **23**, 804 (2004).

[33] S. Liu and H. Hua, "A systematic method for designing depth-fused multi-focal plane three-dimensional displays," Opt. Express **18**, 11562 (2010).

[34] S. Ravikumar, K. Akeley, and M. S. Banks, "Creating effective focus cues in multi-plane 3D displays," Opt. Express **19**, 20940–20952 (2011).

[35] M. Date, S. Sugimoto, H. Takada, and K. Nakazawa, "Depth-fused 3D (DFD) display with multiple viewing zones," Proc. SPIE **6778**, 677817–677817–8 (2007).

[36] C. Lee, S. DiVerdi, and T. Höllerer, "An immaterial depth-fused 3D display," in "VRST '07," (ACM Request Permissions, New York, New York, USA, 2007), p. 191.

[37] J. Hong, Y. Kim, H.-J. Choi, J. Hahn, J.-H. Park, H. Kim, S.-W. Min, N. Chen, and B. Lee, "Three-dimensional display technologies of recent interest: principles, status, and issues," Appl. Opt. **50**, H87–H115 (2011).

[38] D. Fattal, Z. Peng, T. Tran, S. Vo, M. Fiorentino, J. Brug, and R. G. Beausoleil, "A multi-directional backlight for a wide-angle, glasses-free three-dimensional display," Nature **495**, 348–351 (2013).

[39] B. T. Schowengerdt and E. J. Seibel, "True 3-D scanned voxel displays using single or multiple light sources," J. Soc. Inf. Disp. **14**, 135–143 (2006).

[40] D. Gabor, "A new microscopic principle," Nature **161**, 777–778 (1948).

[41] D. E. Smalley, Q. Y. J. Smithwick, V. M. Bove, J. Barabas, and S. Jolly, "Anisotropic leaky-mode modulator for holographic video displays," Nature **498**, 313–317 (2013).

[42] S.-g. Park, J.-H. Kim, and S.-W. Min, "Polarization distributed depth map for depth-fused three-dimensional display," Opt. Express **19**, 4316 (2011).

[43] S. Jung, J.-H. Park, H. Choi, and B. Lee, "Wide-viewing integral three-dimensional imaging by use of orthogonal polarization switching," Appl. Opt. **42**, 2513–2520 (2003).

[44] J. Hong, J.-H. Park, S. Jung, and B. Lee, "Depth-enhanced integral imaging by use of optical path control," Opt. Lett. **29**, 1790–1792 (2004).

[45] A. Jones, I. McDowall, H. Yamada, M. Bolas, P. Debevec, I. McDowall, and H. Yamada, "Rendering for an interactive 360 light field display," ACM Transactions on Graphics (TOG) **26**, 40 (2007).

[46] P. Yeh and C. Gu, *Optics of Liquid Crystal Displays* (John Wiley & Sons, 2010).

[47] D. Armitage, I. Underwood, and S.-T. Wu, *Introduction to Microdisplays* (John Wiley & Sons, 2006).

[48] M. S. Brennesholtz and E. H. Stup, *Projection Displays* (Jone Wiley & Sons, 2008).

[49] W. Fleming, "Vertical three-dimensional image screen," US Patent Office (1987).

[50] H. Urey, K. V. Chellappan, E. Erden, and P. Surman, "State of the art in stereoscopic and autostereoscopic displays," Proc. IEEE **99**, 540–555 (2011).

[51] S. Suyama, H. Sonobe, T. Soumiya, A. Tsunakawa, H. Yamamoto, and H. Kuribayashi, "Edge-based depth-fused 3D display," in Digital Holography and Three-Dimensional Imaging (2013), (Optical Society of America, Washington, D.C., 2013), p. DM2A.3.

[52] S. Suyama, Y. Ishigure, H. Takada, and K. Nakazawa, "Evaluation of visual fatigue in viewing a depth-fused 3-D display in comparison with a 2-D display," NTT Tech. Rev. **3**, 82–89 (2005).

[53] J.-W. Seo and T. Kim, "Double-layer projection display system using scattering polarizer film," Jpn. J. Appl. Phys. **47**, 1602–1605 (2008).

[54] E. Walton, A. Evans, G. Gay, A. Jacobs, T. Wynne Powell, G. Bourhill, P. Gass, and H. Walton, "P-74: Seeing Depth from a Single LCD," SID Symposium Digest of Technical Papers **40**, 1395–1398 (2009).

[55] S.-g. Park, J.-H. Jung, Y. Kim, and B. Lee, "Depth-fused display with enhanced viewing region," in Biomedical Optics and 3-D Imaging (2012), OSA (Optical Society of America, Miami, FL, USA, 2012), p. DSu1C.5.

[56] S.-g. Park, J.-H. Jung, and B. Lee, "Depth expansion of depth-fused display based on integral imaging method," in IMID 2012, (KIDS, Daegu, Korea, 2012), pp. 473–474.

[57] J.-H. Jung, J. Yeom, J. Hong, K. Hong, S.-W. Min, and B. Lee, "Effect of fundamental depth resolution and cardboard effect to perceived depth resolution on multi-view display," Opt. Express **19**, 20468–20482 (2011).

[58] J.-Y. Son, V. V. Saveljev, Y.-J. Choi, J.-E. Bahn, S.-K. Kim, and H. Choi, "Parameters for designing autostereoscopic imaging systems based on

lenticular, parallax barrier, and integral photography plates," Opt. Eng **42**, 3326–3333 (2003).

[59] S.-W. Min, J. Kim, and B. Lee, "New characteristic equation of three-dimensional integral imaging system and its applications," Jpn. J. Appl. Phys. **44**, L71–L74 (2005).

[60] F. Wu, H. Deng, C.-G. Luo, D.-H. Li, and Q.-H. Wang, "Dual-view integral imaging three-dimensional display," Appl. Opt. **52**, 4911–4914 (2013).

[61] Y. Kim, G. Park, J.-H. Jung, J. Kim, and B. Lee, "Color moiré pattern simulation and analysis in three-dimensional integral imaging for finding the moiré-reduced tilted angle of a lens array," Appl. Opt. **48**, 2178–2187 (2009).

[62] V. Saveljev and S.-K. Kim, "Simulation and measurement of moiré patterns at finite distance," Opt. Express **20**, 2163–2177 (2012).

[63] X. Hu and H. Hua, "High-resolution optical see-through multi-focal-plane head-mounted display using freeform optics," Opt. Express **22**, 13896–13903 (2014).

[64] S.-g. Park, J. Yeom, Y. Jeong, N. Chen, J.-Y. Hong, and B. Lee, "Recent issues on integral imaging and its applications," J. Inf. Disp. **15**, 37–46 (2014).

[65] Y. Takaki and N. Nichiyo, "Multi-projection of lenticular displays to construct a 256-view super multi-view display," Opt. Express **18**, 8824–8835 (2010).

[66] S.-K. Kim, D.-W. Kim, Y. M. Kwon, and J.-Y. Son, "Evaluation of the monocular depth cue in 3D displays," Opt. Express **16**, 21415 (2008).

[67] Y. Takaki, Y. Urano, S. Kashiwada, H. Ando, and K. Nakamura, "Super multi-view windshield display for long-distance image information presentation," Opt. Express **19**, 704–716 (2011).

[68] S.-g. Park, J.-H. Jung, Y. Jeong, and B. Lee, "Depth-fused display with improved viewing characteristics," Opt. Express **21**, 28758–28770 (2013).

[69] G. Park, J.-H. Jung, K. Hong, Y. Kim, Y.-H. Kim, S.-W. Min, and B. Lee, "Multi-viewer tracking integral imaging system and its viewing zone analysis," Opt. Express **17**, 17895–17908 (2009).

[70] Z.-L. Xiong, Q.-H. Wang, S.-L. Li, H. Deng, and C.-C. Ji, "Partially-overlapped viewing zone based integral imaging system with super wide viewing angle," Opt. Express **22**, 22268–22277 (2014).

[71] D. Leithinger, D. Lakatos, A. DeVincenzi, M. Blackshaw, and H. Ishii, "Direct and gestural interaction with relief," in UIST '11, (ACM Press, New York, New York, USA, 2011), p. 541.

[72] M. Hirsch, S. Izadi, H. Holtzman, and R. Raskar, "8D: Interacting with a relightable glasses-free 3D display," in CHI '13, (ACM Press, Paris, France, 2013), p. 2209.

[73] B. Long, S. A. Seah, T. Carter, and S. Subramanian, "Rendering volumetric haptic shapes in mid-air using ultrasound," ACM Transactions on Graphics (TOG) **33**, 181–10 (2014).

초록

이 논문에서는 투사형 디스플레이 또는 집적 영상 디스플레이 기술을 적용하여, 깊이 융합 디스플레이의 관찰 특성을 향상시키기 위한 다양한 방법들을 제안한다. 깊이 융합 디스플레이는 체적형 3차원 디스플레이의 한 종류로, 다층의 깊이 단층 영상으로 이루어져있다. 관찰자의 시축(視軸)에 위치한 각각의 영상에 적절한 밝기 비율을 적용하면, 디스플레이 층 사이의 공간에 연속적인 초점 변화를 유발하는 것이 가능하다. 이러한 부피 표현 특성으로 인하여 깊이 융합 디스플레이는 매우 자연스러운 3차원 영상을 구현하는 것이 가능하다. 하지만 기초 영상들이 시선축 상의 정확하게 위치해야만 영상들이 정확하게 합쳐지게되며, 그렇지 않으면 영상들이 연속적인 부피영상이 아닌 분리된 평면 영상으로 관찰되게 된다. 이러한 관찰 특성을 깊이 융합 디스플레이의 관찰 조건을 매우 까다롭게 제한하며, 응용 범위를 제한하는 결과를 가져왔다. 깊이 융합 디스플레이를 구성하는 단층 면들을 증가시킴으로서 영상의 부피화소화함으로써 시야각이나 깊이 범위를 상승시키는 것이 가능하지만, 그러한 방법은 기하급수적으로 증가하는 시스템의 부피화소의 개수에 따라 시스템의 복잡도가 매우 증가하게 되는 단점이 있다. 이러한 문제를 해결하기 위하여, 상대적으로 간단한 시스템 구조를 적용하는 하이브리드 깊이 융합 디스플레이방식을 제안한다. 하이브리드 방식은 깊이 융합 디스플레이에 투사형 디스플레이 또는 무안경식 3차원 디스플레이 기술을 적용하는 방식을 말한다. 투사형 디스플레이 방식은 편광변조된 깊이 정보 방식과 함께 적용되어 3차원 영상 정보를 투사시키는데 이용될 수 있다. 이 때 깊이 정보는 편광 상태를 통해 전달되기 때문에, 공간해상도 또는 영상 재생률의 저하없이 3차원 영상을 재현하는 것이 가능하다. 이러한 편광복조된 깊이 영상은 편광 선택적 확산판을 이용하여 입력된 특정 깊이의 위치에서 상이 맺히게 되며 깊이 융합 효과를 이용해 3차원 영상으로 복원된다. 영상을 복원 하기 위해서 어떠한 능동적인 장치가 필요하지

않기때문에, 기존의 투사형 디스플레이과 마찬가지로 영상의 투사부와 재생 화면을 완전히 분리해서 구동하는 것이 가능하다. 또한 이러한 투사형 디스플레이의 특징으로 인하여 영상의 크기를 쉽게 조절할 수 있으며, 이를 통하여 대화면 시스템 구현을 통한 몰입감 있는 3차원 경험을 제공할 수 있다. 관찰자의 위치 변화로 인한 시축 변화는 기초 영상의 어긋남을 야기하게 된다. 이러한 영상의 어긋남은 시축의 변화에 맞추어 기초 영상을 이동시켜줌으로써 보상해 줄 수 있다. 이것은 다시점 방식을 적용하여 구현하는 것이 가능하다. 일반적인 다시점 영상이 관찰 시점에 따라서 새로운 시점 영상을 보여주는 것과 달리 시축 변화에 맞추어 이동된 깊이 융합 영상의 기초 영상을 보여주면, 관찰자는 올바르게 정렬된 3차원 영상을 관찰하게 된다. 또다른 하이브리드 방식은 깊이 융합 디스플레이에 영상 부양법을 적용하는 것이다. 볼록 렌즈와 같은 광학 소자는 물체의 위치를 광학적으로 새로운 깊이로 옮기는 것이 가능하다. 이러한 원리를 기반으로, 관찰자가 인식하는 3차원 영상의 광학적인 깊이가 실제 디스플레이의 간격을 넘어서는 디스플레이를 구현하는 것이 가능하다. 초점 거리가 짧은 렌즈를 이용할 수록 디스플레이 시스템의 부피를 작게 만드는 것이 가능하며, 실질적인 시스템의 구현을 위해서는 렌즈 배열을 이용하는 집적 영상을 통해 적용하는 것이 바람직하다. 영상 부양법을 통해 생성된 영상은 디스플레이 시스템의 뒤쪽이나 앞쪽에 위치할 수 있다. 두 경우 모두 실제 디스플레시스템의 부피보다 확장된 영상 범위를 가질수 있다. 영상이 시스템 앞에 위치한 실상 조건에서는 재생되는 영상과 사용자가 디스플레이의 방해 없이 직접적으로 상호작용 하는 것이 가능하다. 또한 관찰자 추적 시스템을 추가적으로 적용하면, 추가적으로 동적 시차를 줄 수 있으며, 관찰자의 방향에 맞추어 영상을 실시간으로 이동 시켜줌으로써, 시야각을 향상 시키는 것이 가능하다. 본 논문의 각각의 장에서는 앞서 언급한 하이브리드 방법에 대한 기술적인 배경을 설명하고, 실험용 시스템을 통하여 제안된 방법의 구현 가능성을 확인하였다.

주요어: 무안경식 3차원 디스플레이, 깊이 융합 디스플레이, 투사형 디스플레이, 편광 변조, 집적 영상, 다시점 디스플레이, 초점 조절 반응, 관찰자 추적

학번: 2011-30233